

Hierarchical Skeleton Meta-Prototype Contrastive Learning with Hard Skeleton Mining for Unsupervised Person Re-Identification

Haocong Rao^{1,2}, Cyril Leung^{2,3} and Chunyan Miao^{1,2*}

¹School of Computer Science and Engineering, Nanyang Technological University, Singapore.

²Joint NTU-UBC Research Centre of Excellence in Active Living for the Elderly (LILY), Nanyang Technological University, Singapore.

³Department of Electrical and Computer Engineering, The University of British Columbia, Canada.

*Corresponding author(s). E-mail(s): ascymiao@ntu.edu.sg;
Contributing authors: haocong001@ntu.edu.sg; cleung@ece.ubc.ca;

Abstract

With rapid advancements in depth sensors and deep learning, skeleton-based person re-identification (re-ID) models have recently achieved remarkable progress with many advantages. Most existing solutions learn single-level skeleton features from body joints with the assumption of equal skeleton importance, while they typically lack the ability to exploit more informative skeleton features from various levels such as limb level with more global body patterns. The label dependency of these methods also limits their flexibility in learning more general skeleton representations. This paper proposes a generic unsupervised Hierarchical skeleton Meta-Prototype Contrastive learning (Hi-MPC) approach with Hard Skeleton Mining (HSM) for person re-ID with *unlabeled* 3D skeletons. Firstly, we construct hierarchical representations of skeletons to model *coarse-to-fine* body and motion features from the levels of body joints, components, and limbs. Then a hierarchical meta-prototype contrastive learning model is proposed to cluster and contrast the most typical skeleton features (“*prototypes*”) from different-level skeletons. By converting original prototypes into *meta-prototypes* with multiple homogeneous transformations, we induce the model to learn the inherent consistency of prototypes to capture more effective skeleton features for person re-ID. Furthermore, we devise a hard skeleton mining mechanism to adaptively infer the informative importance of each skeleton, so as to focus on harder skeletons to learn more discriminative skeleton representations. Extensive evaluations on five datasets demonstrate that our approach outperforms a wide variety of state-of-the-art skeleton-based methods. We further show the general applicability of our method to cross-view person re-ID and RGB-based scenarios with estimated skeletons.

Keywords: Skeleton-based person re-identification, Unsupervised representation learning, Meta-prototype contrastive learning, Hard skeleton mining

1 Introduction

Person re-identification (re-ID) is a pattern recognition task that aims to retrieve and match a certain pedestrian across different views or occasions. Recent years have witnessed its great success in many applications such as intelligent video surveillance, security authentication, human tracking, and robotics [1–13]. With the surging popularity of low-cost, non-invasive, and accurate skeleton-tracking sensors (*e.g.*, Kinect [14]), person re-ID via 3D skeletons has attracted increasing attention in both academia and industry [15–27], while many important topics of skeleton-based person re-ID (*e.g.*, how to improve both accuracy and scalability) still remain to be studied [25, 28]. In contrast to conventional methods that utilize visual human appearances and body textures from RGB or depth images [29–35], skeleton-based person re-ID models provide numerous advantages such as (1) smaller data size with concise 3D human body representation (*i.e.*, 3D coordinates of key body joints), (2) better privacy protection *without* using appearance information, (3) more robust performance under scale, view, and background variations [22, 36].

Traditional skeleton-based methods [15–19] typically extract hand-crafted features like skeleton descriptors in terms of pre-defined anthropometric and gait attributes of body. Nevertheless, these methods rely heavily on domain expertise such as anatomy and kinematics [37] to model skeleton data, and lack the flexibility to fully exploit latent features beyond human cognition. Recent mainstream methods [20–26] resort to deep neural networks (DNNs) to perform skeleton representation learning. Despite the great efforts, they usually require manually-annotated skeleton data to train or fine-tune models, which is labor-expensive and could reduce their general applicability in practice. Another crucial shortcoming of these methods is that they typically learn skeleton features from a single level (*e.g.*, body joint level [21, 22]) and assume that each skeleton is equally important in representing the patterns of a person [22, 25]. This intrinsically limits their ability to exploit key features of more informative skeletons. For instance, there usually exist skeletons that are either harder to be recognized as the same identity (*i.e.*, large intra-class variations) or easier to be misidentified among different individuals

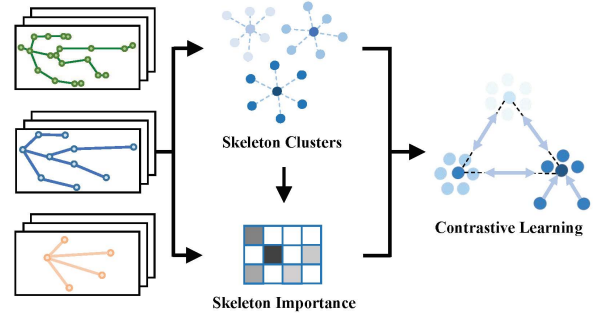


Fig. 1 Our approach hierarchically clusters skeleton representations to infer their inherent importance, and contrasts the key clustered features with the most typical ones to learn effective skeleton representations for unsupervised person re-ID.

(*i.e.*, small inter-class variations), both of which should be given greater attention for learning more effective skeleton representations.

To solve the aforementioned challenges for *unsupervised skeleton-based* person re-ID, we propose a generic Hierarchical skeleton Meta-Prototype Contrastive learning (Hi-MPC) approach with a Hard Skeleton Mining (HSM) mechanism, as shown in Fig. 1. The approach exploits *unlabeled* hierarchical representations of key informative skeletons to contrast and learn the most typical skeleton features for person re-ID. Firstly, we construct a hierarchical representation for each skeleton with coarse-to-fine body partitions, which enables the model to explore body structures and pattern information from different levels. Secondly, a Hierarchical skeleton Meta-Prototype Contrastive learning (Hi-MPC) approach is devised to cluster and contrast the most representative skeleton features (defined as “*prototypes*”) from *different-level* skeleton representations (defined as “*instances*”). To encourage learning more consistent and representative skeleton prototypes, we propose to transform original instances into multiple *homogeneous meta-instances*, and maximize their inherent similarity to corresponding *meta-prototypes* while maximizing their dissimilarity to others, so as to capture discriminative skeleton features and class-related semantics (*e.g.*, intra-class similarity) from various levels of unlabeled skeletons. Thirdly, considering that different skeletons usually possess varying informative value, *e.g.*, some skeletons are more difficult to be classified to the correct identity (defined as “*hard skeletons*”) but

can provide more informative clues for model learning [38], we *for the first time* devise a Hard Skeleton Mining (HSM) mechanism to adaptively infer the importance of each skeleton in learning hard and easily-confused patterns. In this way, HSM enables our model to mine and focus on hard skeletons in Hi-MPC to encourage more effective skeleton representation learning. Lastly, we propose to construct the novel Multi-level Skeleton Meta-Representation (MSMR) that combines skeleton features learned from different levels as the final representation for person re-ID. As a byproduct of our approach, we reveal the feasibility of exploiting more concise and abstract skeleton representations to perform person re-ID.

Our contributions are summarized as follows:

- We devise hierarchical representations of 3D skeletons and propose a novel hierarchical skeleton meta-prototype contrastive learning approach with a hard skeleton mining mechanism to learn effective representations from *unlabeled* skeleton sequences for person re-ID.
- We propose the Hierarchical skeleton Meta-Prototype Contrastive learning (Hi-MPC) that hierarchically contrasts representative features and inherent similarity of different-level skeleton representations to learn discriminative features and high-level semantics for person re-ID.
- We devise a Hard Skeleton Mining (HSM) mechanism to adaptively infer informative importance of skeletons within each sequence to encourage learning more effective skeleton representations from harder skeletons.
- We empirically validate the effectiveness of each level skeleton representation learned from the proposed approach, and combine them to construct the novel Multi-level Skeleton Meta-Representation (MSMR) for person re-ID.
- Extensive experiments on five public benchmarks demonstrate that our approach outperforms most state-of-the-art methods on person re-ID tasks. We further show that our method is generally effective in multi-view and RGB-based scenarios with estimated skeletons.

The rest of this paper is organized as follows. Sec. 2 introduces relevant works on skeleton-based person re-identification and contrastive learning. Sec. 3 describes technical components of the proposed approach. Sec. 4 provides experimental details and a comprehensive comparison between

our approach and existing state-of-the-art methods. Sec. 5 details our ablation study and empirical analysis of the proposed approach. Sec. 6 concludes this paper.

2 Related Works

2.1 Skeleton-Based Person Re-Identification

2.1.1 Hand-Crafted Methods

Most conventional methods manually extract 3D skeleton features from anthropometric and gait aspects to depict human body and motion patterns [16–19]. In [17], seven Euclidean distances between certain joints are integrated into a learnable distance matrix for person re-ID. They are further extended into 13 (denoted as D_{13}) and 16 skeleton descriptors (denoted as D_{16}) in [16] and [19] respectively, which are learned by different classifiers (k -nearest neighbor, support vector machine or Adaboost) to perform person re-ID tasks. Due to the limited performance of existing descriptors and their inherent requirement of domain expertise, these methods are usually combined with more efficient features such as 3D point clouds [15] or face descriptors [19] to boost accuracy. In our work, three representative hand-crafted descriptors (*i.e.*, non-model-based methods), including D_{13} [16], D_{16} [19], and the PoseGait descriptor (denoted as D_{PG}) in [20] that combines pose features, joint angles, limb lengths, and joint motion are compared with deep learning based models.

2.1.2 Deep Learning Based Methods

Recent years have witnessed the great success of deep learning in supervised and self-supervised skeleton representation learning [20–25]. In [20], a CNN-based architecture PoseGait is leveraged to learn 81 pre-defined skeleton/pose features (D_{PG}) for supervised human recognition. A self-supervised skeleton encoding model (AGE) with locality-aware attention based LSTM [21] is devised to encode discriminative gait patterns for person re-ID. Its extension SGELA [22] further enhances self-supervised skeleton semantic learning with diverse skeletal pretext tasks (*e.g.*, time series forecasting [39]) and inter-sequence contrastive mechanisms for the person re-ID task.

Skeleton graphs are constructed in [23] based on the physical connections of body joints or parts to learn skeletal relations and high-level motion semantics via graph attention networks [40] for person re-ID. In [24], multi-scale skeleton reconstruction and cross-scale skeleton inference are further integrated into a graph encoding framework for self-supervised person re-ID. The SimMC framework [25] performs single-level prototype contrastive learning and intra-sequence similarity learning with randomly masked skeleton sequences to realize unsupervised person re-ID. The skeleton/pose data are also utilized in many image/video-based person re-ID methods to help extract pre-defined local/hierarchical body parts [41, 42], disentangle semantic components (*e.g.*, bone locations) [43, 44] or generate pose augmented representations [45]. The key differences between these methods and our approach are two-fold. First, they use skeleton data as *auxiliary* information to combine with RGB images to boost the model performance, while our work exploits only unlabeled skeleton data without using any appearance-based features for person re-ID. Second, they typically leverage the hierarchical structure of the original body skeletons to generate image-based body parts, our approach hierarchically constructs skeleton representations at different levels, each of which corresponds to a new *independent* body representation to learn discriminative pattern information for person re-ID.

Compared to previous hand-crafted, supervised, and self-supervised skeleton-based models, our approach requires no pre-defined skeleton descriptors, graph modeling or pretext design for skeleton representation learning. Our unsupervised method can efficiently exploit *unlabeled* 3D skeleton data to hierarchically mine the most representative features from different-level skeleton representations, which enables capturing comprehensive body patterns and coarse-to-fine skeleton semantics for person re-ID tasks. This work is the first exploration of potential hard skeletons to exploit more informative patterns, and it can be seamlessly integrated into unsupervised contrastive learning to enhance discriminative feature mining.

2.2 Contrastive Learning

Contrastive learning has recently driven various self-supervised and unsupervised paradigms [22, 46–52] to learn efficient data representations in a way of pulling together positive representation pairs and pushing apart negative ones in a certain feature space. An instance discrimination method with exemplar tasks and noise-contrastive estimation (NCE) [53] is proposed in [46] for visual contrastive learning. A context auto-encoding task with probabilistic contrastive loss, InfoNCE, is utilized in the contrastive predictive coding (CPC) model [47] to learn effective representations from different domains. The mini-batch negative sampling mechanism [49] and momentum-based encoder [48] are devised to improve the capacity and consistency of contrastive paradigms, while a Siamese architecture is further explored in [50] to perform contrastive representation learning without using negative pairs or momentum encoders. In [51], contrastive learning and k -means clustering are integrated into a framework for unsupervised visual learning.

Fundamentally different from previous studies that leverage augmented samples of images as contrastive instances, our work devises a new generic meta-prototype contrastive learning paradigm for 3D skeleton data, and exploits unlabeled hierarchical skeleton representations as instances to mine the most representative and discriminative features (*i.e.*, skeleton prototypes) for instance-prototype contrastive learning. In contrast to existing skeleton contrastive learning methods [22, 25], we explore the hierarchical contrastive learning of multi-level skeleton representations, and propose the meta-transformation of instances and prototypes to enhance the inherent consistency and effectiveness of prototype learning. Our approach requires neither extra sampling scheme nor memory mechanism, while it can fully exploit skeletal importance to enhance the contrastive learning of harder and more informative samples to achieve more effective skeleton representations.

2.2.1 Hard Negative Mining for Contrastive Learning

Hard negative mining aims to find more informative training samples that are difficult to discriminate (*e.g.*, easily-confused negatives), which has been widely applied to various areas to accelerate

network training and improve model performance [38, 54–61]. In contrastive learning, existing hard negative mining models can be mainly grouped into (1) *adversarial learning based methods* [55, 56] that generate hard negatives by adversarial optimization and (2) *mixing based methods* [57–59] that mix the negative samples and positive samples in the feature space. In [55], a representation network and its negative adversary are alternately trained to generate the hardest negative samples for contrasting, while [56] further introduces a diversity loss to generate diverse challenging negative samples with different noise. A hard negative mixing strategy is proposed in [57] to mix features of hardest negatives and its query to enhance contrastive learning. To improve the difficulty of generated negatives, a diversity objective function is devised in [59] to mix multiple samples with dynamic weights. Some recent works also explore controllable hard negative mining with an importance sampling strategy [60] or dynamic curriculum learning [61].

Different from previous methods that require extra triplet constraint [38, 62], adversarial learning [55, 56] or sample mixing [57–59], the proposed hard skeleton mining mechanism can directly exploit the inherent similarity between skeleton representations (meta-instance) and cluster-level representations (meta-prototypes) to adaptively infer the informative importance of skeletons at different skeleton levels and different feature subspaces, and mine both hard positive and negative skeleton samples from sequences without using any labels. Our approach is specifically designed to mine key informative skeletons within each sequence, which can be generally applied to different level skeleton representations to enhance the proposed hierarchical contrastive learning for unsupervised skeleton-based person re-ID tasks.

3 The Proposed Approach

The goal of our approach is to perform *unsupervised* person re-identification with unlabeled 3D skeleton sequences. Formally, we denote a sequence of 3D skeletons as $\mathbf{S}_{1:F} = (\mathbf{S}_1, \dots, \mathbf{S}_F) \in \mathbb{R}^{F \times K}$, where $\mathbf{S}_i \in \mathbb{R}^K$ is the i^{th} skeleton with 3D positions of J body joints and $K = 3 \times J$. The training set $\Phi^T = \{\mathbf{S}_{1:F}^{T,i}\}_{i=1}^{N_1}$, probe set $\Phi^P =$

$\{\mathbf{S}_{1:F}^{P,i}\}_{i=1}^{N_2}$, and gallery set $\Phi^G = \{\mathbf{S}_{1:F}^{G,i}\}_{i=1}^{N_3}$ contain N_1 , N_2 , and N_3 skeleton sequences of different persons in varying views or occasions. Each skeleton sequence $\mathbf{S}_{1:F}$ corresponds to a unique identity $y \in \{1, \dots, I\}$ where I is the number of different identities. Our approach aims at learning to encode Φ^P and Φ^G into effective skeleton representations $\{\mathbf{V}_i^P\}_{i=1}^{N_2}$ and $\{\mathbf{V}_j^G\}_{j=1}^{N_3}$ *without using any label*, such that the representation \mathbf{V}_i^P in the probe set can match the representation \mathbf{V}_j^G of the same identity in the gallery set. The overview of our approach is presented in Fig. 2, and we detail each technical component below.

3.1 Hierarchical Skeleton Representations

The human body can be naturally modeled with several key functional regions at different levels (*e.g.*, joints, limbs) [23, 63], which could *hierarchically* characterize different anthropometric or kinetic features of the body. Inspired by this fact, we spatially divide each human skeleton into various non-overlapping partitions, each of which corresponds to a certain body part at the level of joints, body components (*e.g.*, hands) or limbs (*e.g.*, upper limbs). Then we generate the position of each body part by computing the centroid of body joints within the corresponding partition. As presented in Fig. 2, we build hierarchical skeleton representations for each skeleton \mathbf{S} from three levels, namely *joint-level*, *component-level*, and *limb-level* skeleton representations, which can correspondingly contain low, middle, and high level body structures and pattern information of a skeleton. Formally, the l^{th} level representation $\hat{\mathbf{S}}^l \in \mathbb{R}^{3 \times n_l}$ ($l \in \{1, 2, 3\}$) consists of 3D positions of n_l body partitions, where $n_1 = J$, $n_2 = 10$, $n_3 = 5$ correspond to joint-level ($\hat{\mathbf{S}}^1$), component-level ($\hat{\mathbf{S}}^2$), limb-level skeleton representations ($\hat{\mathbf{S}}^3$), respectively. We denote the hierarchical representations of each input skeleton sequence $\mathbf{S}_{1:F}$ as $\hat{\mathbf{S}}_{1:F}^1 \in \mathbb{R}^{F \times 3n_1}$, $\hat{\mathbf{S}}_{1:F}^2 \in \mathbb{R}^{F \times 3n_2}$, and $\hat{\mathbf{S}}_{1:F}^3 \in \mathbb{R}^{F \times 3n_3}$.

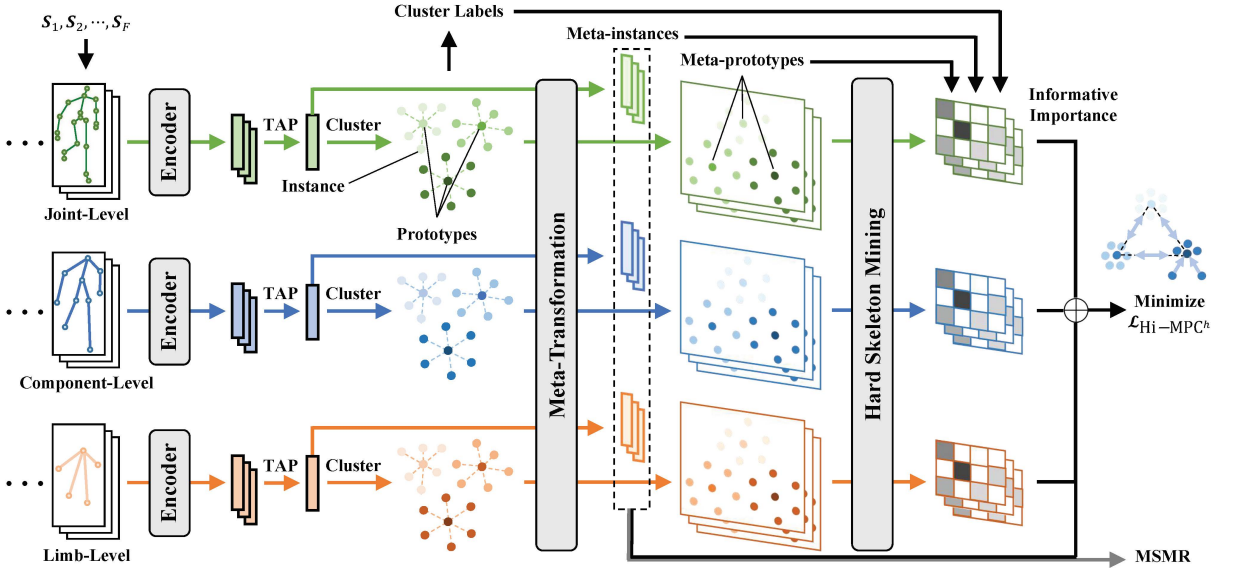


Fig. 2 Schematics of our approach. Firstly, each skeleton sequence S_1, S_2, \dots, S_F is hierarchically represented at joint-level (top), component-level (middle), and limb-level (bottom). Secondly, we perform temporal average pooling (TAP) on the encoded skeleton representations of each level to generate skeleton instances, and cluster them to find prototypes, which are then transformed into meta-instances and meta-prototypes in different contrastive subspaces. Lastly, a hard skeleton mining mechanism (illustrated in Fig. 3) is employed to infer informative importance of skeletons within each sequence, which is integrated into the contrastive loss $\mathcal{L}_{\text{Hi-MPC}^h}$ to enhance the similarity of key meta-instances belonging to the same meta-prototype while maximizing their dissimilarity to other meta-prototypes. The meta-instances learned from different levels are combined to construct multi-level skeleton meta-representation (MSMR) for the person re-ID task.

3.2 Hierarchical Skeleton Meta-Prototype Contrastive Learning

As each pedestrian’s skeletons typically possess unique identity-associated features in terms of anthropometric attributes (e.g., body part lengths) and walking patterns [64], it is desirable to exploit the *most typical skeleton features* (“*prototypes*”) from skeleton sequences (“*instances*”) to differentiate a given person from others. A straightforward solution is to find the skeleton prototypes, which can represent a unique skeleton attribute or concept belonging to certain identities, by clustering skeleton instances for direct prototype-instance contrastive learning in a *single* feature space [25]. However, the inherent randomness of feature initialization or clustering [51] could induce unstable prototype estimation and inconsistent relational distributions (e.g., prototype-instance relations) when representation spaces vary. Based on the assumption that the global distribution of prototypes should be consistent with the distribution of cluster centroids (referred to as “*prototype-cluster consistency*”,

see Appendix I), we propose to construct different contrastive subspaces that inherit from the original feature space of prototypes to enhance contrastive learning. In particular, we perform prototype-instance contrasting in each *individual* contrastive subspace, which are combined based on the prototype-cluster consistency to encourage more robust probability estimation of prototypes and more consistent contrastive learning. To this end, we devise the **hierarchical skeleton meta-prototype contrastive learning (Hi-MPC)** to homogeneously transform original prototypes and instances into **meta-prototypes** and **meta-instances** at each skeleton level, and contrast their inherent similarity in different transformed contrastive subspaces to *jointly* learn representative discriminative skeleton features for person re-ID.

Given the l^{th} level skeleton representations $\hat{S}_1^l, \dots, \hat{S}_F^l$ of an input skeleton sequence, we first encode them and apply temporal average pooling (TAP) to obtain a sequence-level skeleton

representation, *i.e.*, instance (shown in Fig. 2) as:

$$\mathbf{v}^{l,(i)} = \frac{1}{F} \sum_{j=1}^F \psi^l \left(\hat{\mathbf{S}}_j^{l,(i)} \right) = \frac{1}{F} \sum_{j=1}^F \mathbf{z}_j^{l,(i)}, \quad (1)$$

where $\psi^l(\cdot)$ is the l^{th} level encoder built by a multi-layer perceptron (MLP) network with one hidden layer, $\mathbf{z}_j^{l,(i)} \in \mathbb{R}^{h_1}$ denotes the encoded features of the l^{th} level representation of j^{th} skeleton in the i^{th} training skeleton sequence, and $\mathbf{v}^{l,(i)} \in \mathbb{R}^{h_1}$ denotes the encoded l^{th} level representation of i^{th} training skeleton sequence $\hat{\mathbf{S}}_1^{l,(i)}, i \in \{1, \dots, N_1\}$. Here we adopt TAP to *average* the temporal dynamics of all skeletons to represent the features of a sequence [25]. It is worth noting that TAP also keeps the consistency of feature dimensions between skeleton-level and sequence-level representations. This allows us to directly compute their inherent similarity by dot products without extra dimension transformation (see Sec. 3.3).

Then, to mine the original skeleton prototypes, we exploit the encoded sequence-level representations $\mathbb{V}^l = \{\mathbf{v}^{l,(1)}, \dots, \mathbf{v}^{l,(N_1)}\}$ as skeleton instances, and leverage the DBSCAN algorithm [65] to cluster instances of similar features and semantics. As shown in Fig. 2, we generate clusters as $\hat{\mathbb{V}}_c^l = \{\mathbf{v}_{c,k}^l\}_{k=1}^{n_c}, c \in \{1, \dots, C\}$, where C denotes the number of different clusters, *i.e.*, pseudo classes, and the c^{th} cluster $\hat{\mathbb{V}}_c^l$ contains n_c instances. Note that we perform clustering *individually* on each level of hierarchical skeleton representations to better capture different level semantics and retain coarse-to-fine skeleton features. The instance features of the same cluster are averaged as the corresponding skeleton prototype with:

$$\mathbf{p}_c^l = \frac{1}{n_c} \sum_{k=1}^{n_c} \mathbf{v}_{c,k}^l, \quad (2)$$

where $\mathbf{p}_c^l \in \mathbb{R}^{h_1}$ denotes the original skeleton prototype of the c^{th} cluster $\hat{\mathbb{V}}_c^l$ generated from the l^{th} level skeleton instances. Given the original prototypes and instances, our model converts them into *meta-prototypes* and *meta-instances* with multiple meta-transformation heads by:

$$(\hat{\mathbf{v}}_{c,k}^l)^m = \mathbf{H}_1^{l,m} \mathbf{v}_{c,k}^l, \quad (3)$$

$$(\hat{\mathbf{p}}_c^l)^m = \mathbf{H}_2^{l,m} \mathbf{p}_c^l, \quad (4)$$

where $(\hat{\mathbf{v}}_{c,k}^l)^m, (\hat{\mathbf{p}}_c^l)^m \in \mathbb{R}^{h_2}$ denote the m^{th} meta-instance and meta-prototype transformed from $\mathbf{v}_{c,k}^l$ and \mathbf{p}_c^l . Here $\mathbf{H}_1^{l,m}, \mathbf{H}_2^{l,m} \in \mathbb{R}^{h_2 \times h_1}$ are corresponding learnable weight matrices of the m^{th} transformation head. $m \in \{1, \dots, M\}$ and M denotes the number of different transformation heads. Considering that both original instances and prototypes come from the same domain, *i.e.*, being represented in the *homogeneous* feature space of the same dimension [66], it is natural to employ homogeneous feature mapping for each pair of heads (defined as “*meta-transformation heads*”) with $\mathbf{H}_1^{l,m} = \mathbf{H}_2^{l,m}$ and $h = h_1 = h_2$. The meta-transformation heads map both instances and prototypes into the *same* m^{th} new feature space, which can be viewed as the m^{th} subspace *linearly* transformed from the original contrastive feature space, to generate homogeneous meta-instances and meta-prototypes. It should be noted that we do NOT use *heterogeneous* feature mapping (*i.e.*, $\mathbf{H}_1^{l,m} \neq \mathbf{H}_2^{l,m}$), as it separately maps instances and prototypes into two different feature subspaces with domain shifts [67] and degrades the model performance (see Appendix II).

To jointly focus on representative skeleton features of all meta-prototypes and capture different-level skeleton semantics (*e.g.*, class-related patterns) from diverse contrastive feature subspaces, we propose the Hi-MPC loss below:

$$\mathcal{L}_{\text{Hi-MPC}} = \sum_{l=1}^3 \sum_{i=1}^{I_l} \sum_{m=1}^M -\log \frac{\exp \left((\hat{\mathbf{v}}^{l,(i)})^m \cdot (\hat{\mathbf{p}}_+^l)^m / \tau \right)}{\sum_{c=1}^C \exp \left((\hat{\mathbf{v}}^{l,(i)})^m \cdot (\hat{\mathbf{p}}_c^l)^m / \tau \right)}, \quad (5)$$

where I_l denotes the number of instances in all clusters generated from the l^{th} level skeleton representations, $(\hat{\mathbf{v}}^{l,(i)})^m$ denotes the m^{th} transformed meta-instance of i^{th} instance belonging to its corresponding meta-prototype $(\hat{\mathbf{p}}_+^l)^m$, $(\hat{\mathbf{p}}_c^l)^m$ is the meta-prototype of the c^{th} cluster at the l^{th} level, and τ is the temperature for contrastive learning. We set $\tau = \sqrt{h}$ to scale the dot products to improve the stability of contrastive learning [68]. Note that $\mathcal{L}_{\text{Hi-MPC}}$ is averaged over all meta-instances for training. The Hi-MPC approach combining both hierarchical skeleton clustering (see Eq. (1) and (2)) and multiple meta-transformations (see Eq. (3) and (4)) enables our model to perform a coarse-to-fine skeleton prototype estimation and mine different-level skeleton semantics (*e.g.*, identity-specific semantics), and

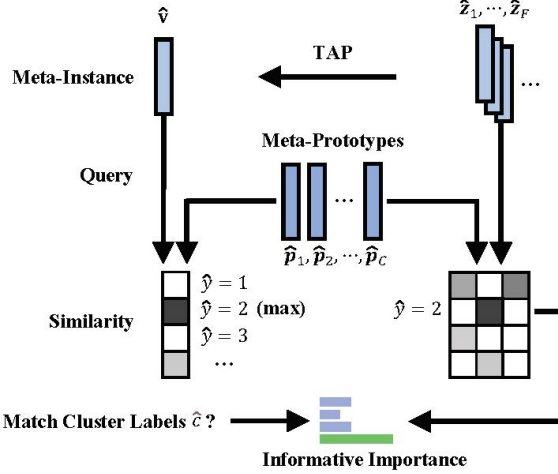


Fig. 3 Computation flow of HSM mechanism. The similarity between skeleton representations $\hat{z}_1, \dots, \hat{z}_F$ and the meta-prototype (\hat{y}) predicted by the meta-instance \hat{v} is first queried. The informative importance is then inferred based on the true or false matching of the cluster label \hat{c} .

also encourages more consistent prototype learning by jointly attending to key meta-prototypes in different representation subspaces. However, Hi-MPC only considers sequence-level skeleton representations, *i.e.*, instances with averaged skeleton features (see Eq. (1)), and cannot fully exploit key skeletons with higher importance in each sequence for contrastive learning, which motivates us to propose the hard skeleton mining mechanism below.

3.3 Hard Skeleton Mining Mechanism

Different skeletons within the same sequence could possess different importance (*referred to as “informative importance”*) in mining hard (*e.g.*, easily-confused) patterns of a person. In particular, similar-looking skeletons and patterns shared among different persons (*referred to as “hard negatives”*), or wildly different poses of the same person (*referred to as “hard positives”*), are typically harder to be distinguished while they can provide more informative clues for models to comprehend the full concept of “same person” [38]. To achieve this goal, we propose the **hard skeleton mining (HSM) mechanism** to encourage the model to focus on skeleton representations with higher informative importance from hard negatives and hard positives in Hi-MPC.

As shown in Fig. 3, given the skeleton sequence representation \hat{v} that belongs to the \hat{c}^{th} cluster, we first predict its label by querying the dot product based similarity with meta-prototypes in the m^{th} contrastive feature subspace by:

$$\hat{y}^m = \arg \max_i ((\hat{v})^m \cdot (\hat{p}_i)^m). \quad (6)$$

In Eq. (6), $\hat{y}^m \in \{1, \dots, C\}$ is the predicted cluster label, $(\hat{v})^m$ and $(\hat{p}_i)^m$ denote the meta-instance and the i^{th} meta-prototype generated by the m^{th} meta-transformation head. It is worth noting that the *cluster label* (denoted as \hat{c}) generated by DBSCAN algorithm is adopted as the ground-truth label since the real label is not available. We use the label of the cluster centroid (*i.e.*, meta-prototype) that has the maximum similarity with $(\hat{v})^m$ as the predicted cluster label of $(\hat{v})^m$ in the m^{th} contrastive feature subspace. For convenience, in Eq. (6) we omit the superscripts of levels and use $\hat{S}_{1:F}$, $(\hat{v})^m$, and $(\hat{p}_i)^m$ to denote the l^{th} level representation $\hat{S}_{1:F}^l$, $(\hat{v}^l)^m$, and $(\hat{p}_i^l)^m$, while \hat{y}^m corresponds to the predicted cluster label of the meta-instance $(\hat{v})^m$.

Having obtained encoded features $\hat{z}_1, \dots, \hat{z}_F$ of F skeletons in $\hat{S}_{1:F}$, where $\hat{z}_j = \psi(\hat{S}_j)$ and $j \in \{1, \dots, F\}$ (see Eq. (1)), we assign the cluster label \hat{y}^m predicted by their sequence-level representation $(\hat{v})^m$ to each of them. As illustrated in Fig. 3, we compute the inherent similarity of each skeleton representation to the predicted cluster using:

$$\delta((\hat{z}_j)^m) = \frac{\exp((\hat{z}_j)^m \cdot (\hat{p}_{\hat{y}^m})^m)}{\sum_{t=1}^F \exp((\hat{z}_t)^m \cdot (\hat{p}_{\hat{y}^m})^m)}. \quad (7)$$

In Eq. (7), $\delta((\hat{z}_j)^m) \in (0, 1)$ represents the *normalized* similarity between the representation of j^{th} skeleton and the meta-prototype corresponding to the predicted \hat{y}^m cluster in the m^{th} contrastive subspace. For clarity and consistency, we use $(\hat{z}_j)^m$ to represent the j^{th} skeleton representation transformed by the m^{th} head corresponding to Eq. (3). $\delta((\hat{z}_j)^m)$ can be interpreted as the the degree of certainty that the j^{th} skeleton within the sequence is classified to \hat{y}^m in the m^{th} feature subspace, while higher certainty indicates that the skeleton is easier for learning to realize correct classification. Hence, the informative importance

Algorithm 1 Main Algorithm of Hi-MPC with HSM

Input: Unlabeled training skeleton sequences $\Phi^T = \left\{ \mathbf{S}_{1:F}^{T,(i)} \right\}_{i=1}^{N_1}$, initialized encoder function $\psi(\cdot)$, initialized M meta-transformation heads $\text{Meta}^m(\cdot)$, temperature τ

Output: Encoder $\psi(\cdot)$, meta-transformation head $\text{Meta}^m(\cdot)$

- 1: $\hat{\mathbf{S}}_{1:F}^{1,(i)}, \hat{\mathbf{S}}_{1:F}^{2,(i)}, \hat{\mathbf{S}}_{1:F}^{3,(i)} = \text{Hier} \left(\mathbf{S}_{1:F}^{T,(i)} \right)$ ▷ Hierarchical skeleton representations at joint/component/limb-level
- 2: **repeat**
- 3: $\mathbf{v}^{l,(i)} = \text{TAP} \left(\psi(\hat{\mathbf{S}}_{1:F}^{l,(i)}) \right) = \text{TAP} \left(\mathbf{z}_1^{l,(i)}, \dots, \mathbf{z}_F^{l,(i)} \right)$ ▷ Encode hierarchical skeleton sequences into instances
- 4: $\{\hat{\mathbb{V}}_c^l\}_{c=1}^C = \text{DBSCAN} \left(\{\mathbf{v}^{l,(i)}\}_{i=1}^{N_1} \right)$ ▷ Find clusters and discard outliers
- 5: $\mathbf{p}_c^l = \text{Proto} \left(\hat{\mathbb{V}}_c^l \right)$ ▷ Generate skeleton prototypes with Eq.(2)
- 6: $((\hat{\mathbf{v}}_{c,k}^l)^m, (\hat{\mathbf{p}}_c^l)^m) = \text{Meta}^m \left(\mathbf{v}_{c,k}^l, \mathbf{p}_c^l \right)$ ▷ Perform the m^{th} meta-transformation with Eq.(3), (4)
- 7: $\hat{y}^m = \text{Pred} \left((\hat{\mathbf{z}}^l)^m \right) = \text{Pred} \left((\hat{\mathbf{v}}^l)^m \right)$ ▷ Predict cluster label for $(\hat{\mathbf{v}}^l)^m$ and its skeletons with Eq.(6)
- 8: Use predicted meta-prototype $(\hat{\mathbf{p}}_{\hat{y}^m})^m$ to infer importance $\bar{\delta} \left((\hat{\mathbf{z}}^l)^m \right)$ of each skeleton with Eq. (8)
- 9: $\mathcal{L}_{\text{Hi-MPC}^h} \left(\bar{\delta} \left((\hat{\mathbf{z}}_j^l)^m \right), (\hat{\mathbf{z}}_j^l)^m, \{(\hat{\mathbf{p}}_c^l)^m\}_{c=1}^C, \tau \right)$ ▷ Compute importance-weighted contrastive loss with Eq.(9)
- 10: Update parameters of $\psi(\cdot)$ and $\text{Meta}^m(\cdot)$ to minimize $\mathcal{L}_{\text{Hi-MPC}^h}$
- 11: **until** *MaxEpoch* or *MaxPatience*

of each skeleton in the same sequence can be inferred by:

$$\bar{\delta}((\hat{\mathbf{z}}_j)^m) = \frac{\exp \left(\mathbb{I}(\hat{y}^m, \hat{c}) \left((\hat{\mathbf{z}}_j)^m \cdot (\hat{\mathbf{p}}_{\hat{y}^m})^m \right) \right)}{\sum_{t=1}^F \exp \left(\mathbb{I}(\hat{y}^m, \hat{c}) \left((\hat{\mathbf{z}}_t)^m \cdot (\hat{\mathbf{p}}_{\hat{y}^m})^m \right) \right)}, \quad (8)$$

where $\bar{\delta}((\hat{\mathbf{z}}_j)^m) \in (0, 1)$ represents the informative importance of the j^{th} skeleton in the sequence $\hat{\mathbf{S}}_{1:F}$ when being represented in the m^{th} contrastive feature subspace, and $\mathbb{I}(\hat{y}^m, \hat{c}) = -1$ if the predicted label \hat{y}^m of $(\hat{\mathbf{z}}_j)^m$ is \hat{c} otherwise $\mathbb{I}(\hat{y}^m, \hat{c}) = 1$. Intuitively, when the label prediction is true, *i.e.*, $\hat{y}^m = \hat{c}$, the hardest positive is the skeleton with the *lowest* certainty $\delta(\cdot)$, which is more likely to contain diverse patterns of the same person and possesses higher informative importance, thus we have $\mathbb{I}(\hat{y}^m, \hat{c}) = -1$ and $\bar{\delta}(\cdot) \propto \frac{1}{\delta(\cdot)}$. When the model fails to predict correctly, *i.e.*, $\hat{y}^m \neq \hat{c}$, the hardest negative is the most certain skeleton being classified to the false label, while it contains more similar information that needs to be carefully distinguished. In this case, we have $\bar{\delta}(\cdot) \propto \delta(\cdot)$, which is naturally achieved with $\mathbb{I}(\hat{y}^m, \hat{c}) = 1$. To facilitate coarse-to-fine pattern learning, the proposed HSM is performed on each level of skeleton hierarchical representations.

To fully exploit skeletons within each sequence and focus on harder skeletons with higher informative importance for Hi-MPC training, we integrate the skeleton importance into contrastive learning by proposing the $\mathcal{L}_{\text{Hi-MPC}^h}$ loss as follows:

$$\mathcal{L}_{\text{Hi-MPC}^h} = \sum_{l=1}^3 \sum_{i=1}^{I_l} \sum_{j=1}^F \sum_{m=1}^M \bar{\delta} \left((\hat{\mathbf{z}}_j^{l,(i)})^m \right) \text{Softmax}_j \left((\hat{\mathbf{z}}_j^{l,(i)})^m \cdot (\hat{\mathbf{p}}_+^l)^m / \tau \right), \quad (9)$$

where $\text{Softmax}_j \left((\hat{\mathbf{z}}_j^{l,(i)})^m \cdot (\hat{\mathbf{p}}_+^l)^m / \tau \right) = \frac{\exp \left((\hat{\mathbf{z}}_j^{l,(i)})^m \cdot (\hat{\mathbf{p}}_+^l)^m / \tau \right)}{\sum_{c=1}^C \exp \left((\hat{\mathbf{z}}_j^{l,(i)})^m \cdot (\hat{\mathbf{p}}_c^l)^m / \tau \right)}$. The proposed $\mathcal{L}_{\text{Hi-MPC}^h}$ in Eq. (9) inherits from $\mathcal{L}_{\text{Hi-MPC}}$ (see Eq. (5)) and combines the proposed HSM mechanism to adaptively infer the informative importance $\bar{\delta}(\cdot)$ of F skeletons in each sequence to enhance the proposed hierarchical skeleton meta-prototype contrastive learning. Instead of directly leveraging sequence-level skeleton representations $\mathbf{v}^{l,(i)}$ for Hi-MPC (see Sec. 3.2), the proposed $\mathcal{L}_{\text{Hi-MPC}^h}$ can take advantage of finer-grained pattern information contained in *each key skeleton* and corresponding hierarchical representations to enhance the Hi-MPC learning (Eq. (5)) to mine more discriminative skeleton features for person re-ID tasks. More details about theoretical and empirical analyses are provided in the appendices.

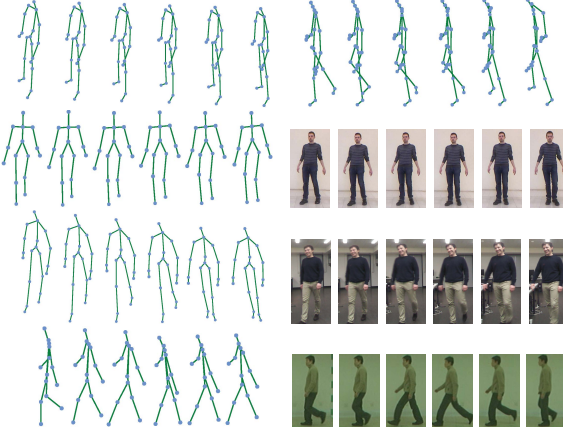


Fig. 4 Examples of 3D skeletons in KGBD (left of 1st row), KS20 (right of 1st row), IAS (2nd row), BIWI (3rd row), and CASIA-B (4th row). We display both skeleton and RGB samples for RGBD datasets (IAS, BIWI). Note: Skeletons of CASIA-B are estimated from RGB images.

3.4 Multi-Level Skeleton Meta-Representation

To combine different-level body and motion semantics embedded in hierarchical skeleton representations and aggregate typical skeleton features learned from different meta-transformed subspaces, we propose to construct ***multi-level skeleton meta-representation (MSMR)*** as the final skeleton representation with:

$$\begin{aligned} \mathbf{V} &= [\mathbf{V}^1; \mathbf{V}^2; \mathbf{V}^3] \\ &= \left[\frac{1}{M} \sum_{m=1}^M (\hat{\mathbf{v}}^1)^m; \frac{1}{M} \sum_{m=1}^M (\hat{\mathbf{v}}^2)^m; \frac{1}{M} \sum_{m=1}^M (\hat{\mathbf{v}}^3)^m \right]. \end{aligned} \quad (10)$$

In Eq. (10), $\mathbf{V}^l \in \mathbb{R}^h$ denotes the l^{th} level skeleton meta-representation that aggregates features of skeleton meta-instances $(\hat{\mathbf{v}}^l)^m$ learned from M meta-transformed subspaces, $[; ;]$ represents feature concatenation, and $\mathbf{V} \in \mathbb{R}^{3h}$ is the proposed MSMR that combines different-level skeleton meta-representations for person re-ID.

3.5 The Entire Approach

The computation flow of our approach can be summarized as: $\mathbf{S} \rightarrow \hat{\mathbf{S}}$ (Sec. 3.1) $\rightarrow \mathbf{v}$ (Sec. 3.2) $\rightarrow \hat{\mathbf{v}}$ $\rightarrow \hat{\mathbf{p}}$ $\rightarrow \hat{\mathbf{y}}^m$ (Sec. 3.3) $\rightarrow \bar{\delta}((\hat{\mathbf{z}}_j)^m) \rightarrow \mathcal{L}_{\text{Hi-MPC}^h}$. As illustrated in Algorithm 1, we perform hierarchical skeleton meta-prototype contrastive learning by minimizing $\mathcal{L}_{\text{Hi-MPC}^h}$, so as to optimize the encoder $\psi(\cdot)$ and meta-transformation heads

Table 1 Overview of datasets (K: thousand). Different testing splits are used for gallery sets and probe sets (see Sec. 4.1). “W”, “S”, “A”, and “B” denote BIWI-Walking, BIWI-Still, IAS-A, and IAS-B testing sets, respectively. “N”, “C”, and “B” represent “Normal”, “Clothes”, and “Bags” conditions of CASIA-B, respectively. Note: The 3D skeletons of CASIA-B are estimated from RGB videos.

# Datasets	KGBD	BIWI	KS20	IAS	CASIA-B
# Train IDs	164	50	20	11	124
# Train Skeletons	188.7K	205.8K	36.0K	89.0K	706.5K
# Probe IDs	164	28	20	11	62
# Probe Skeletons	94.1K	W: 4.9K S: 3.2K	3.3K	A: 7.0K B: 7.8K	N: 162.1K C: 54.4K B: 53.9K
# Gallery IDs	164	28	20	11	62
# Gallery Skeletons	188.7K	W: 4.9K S: 3.2K	3.3K	A: 7.0K B: 7.8K	N: 162.1K C: 54.4K B: 53.9K

to learn effective skeleton representations in an unsupervised manner. During the optimization process, clustering and contrastive learning are alternated to encourage better skeleton representation learning with more reliable clusters. For the person re-ID task, we encode the probe set Φ^P into MSMR, $\{\mathbf{V}_i^P\}_{i=1}^{N_2}$, and match it with corresponding representations, $\{\mathbf{V}_j^G\}_{j=1}^{N_3}$, of the same identity in the gallery set Φ^G using Euclidean distance.

4 Experiments

4.1 Experimental Setup

We validated the effectiveness of our approach on four skeleton-based person re-ID benchmarks: *Kinect Gait Biometry Dataset (KGBD)* [18], *BIWI RGBD-ID Dataset (BIWI)* [16], *KS20 Vis-Lab Multi-View Kinect Skeleton Dataset (KS20)* [69], *IAS-Lab RGBD-ID Dataset (IAS)* [70], and a large-scale RGB video based multi-view gait dataset: *CASIA-B* [71]. The skeleton data in KGBD, BIWI, KS20, and IAS datasets are captured by the depth sensors like Microsoft Kinect [14]. The original CASIA-B dataset does not contain 3D skeleton data, and we follow [20] to exploit pre-trained pose estimation models to extract 3D skeletons from RGB videos of CASIA-B, so as to evaluate the performance of our approach on RGB-estimated skeletons. As detailed in Table 1, these five datasets contain skeleton data of 164, 50, 20, 11, and 124 different identities, respectively.

We follow the commonly-used settings of probe and gallery in the literature [25]: For the BIWI and IAS datasets, as different testing sets are

non-overlapped and contain all pedestrians under different scenes, we evaluate our approach on each testing set by setting it as the probe while the other one is adopted as the gallery. The KGBD dataset contains different skeleton videos (*i.e.*, long skeleton sequences) of each pedestrian with varying numbers of walking rounds. Since no training/testing splits are given, we randomly choose one skeleton video of each person to split skeleton sequences and construct the probe set, and equally divide the remaining videos to build the training set and gallery set. The KS20 dataset collects skeleton data of pedestrians from five different viewpoints, including 0° , 30° , 90° , 130° , and 180° . We employ different splitting setups to evaluate the multi-view person re-ID performance of our approach. For Random View Evaluation (RVE), one sequence is randomly selected from each viewpoint as the probe sequence and the remaining skeleton sequences are equally divided into gallery and training sequences. In Cross-View Evaluation (CVE) setup, we match persons across views, *i.e.*, matching between two different views that are not involved in training. We set sequences from two different viewpoints as the probe set and gallery set, respectively, while adopting sequences from the remaining viewpoints as the training set. The CASIA-B dataset contains sequences of 124 individuals under 11 different views and 3 conditions—pedestrians wearing a bag (“Bags”), wearing a coat (“Clothes”), and without any coat or bag (“Normal”). We follow the person re-ID protocols in [72] to evaluate the proposed skeleton-based approach on CASIA-B. Experiments with each setup are repeated for multiple times and the average performance is reported in this work. More details about the experimental setups are given in Appendix II.

4.2 Implementation Details

The numbers of body joints in skeletons are $J = 25$ for KS20, $J = 20$ for KGBD, BIWI, IAS, and $J = 14$ for CASIA-B. For fair comparison with existing methods, we set the sequence length $F = 6$ on four skeleton-based datasets (KS20, KGBD, BIWI, IAS) and $F = 40$ on estimated skeleton data of CASIA-B. Three level (*i.e.*, joint-level, component-level, limb-level) hierarchical skeleton representations are combined as the final configuration to construct MSMR in

the experiments. The embedding feature size of skeleton representations is $h = 256$, and the number of meta-transformation heads is $M = 8$ for all datasets. We empirically set the maximum distance in the DBSCAN algorithm to 0.6 (KGBD, BIWI-S), 0.8 (KS20, IAS, BIWI-W), 0.75 (CASIA-B), and employ minimum amount of samples with 4 for KGBD and 2 for other datasets. The Adam optimizer is used with learning rate 0.00035 and the batch size is set to 256 on all datasets. We present full implementation details in the appendices and our source code is released at <https://github.com/Kali-Hac/Hi-MPC>.

4.3 Evaluation Metrics

We compute the Cumulative Matching Characteristics (CMC) curve and adopt Rank-1 accuracy (R_1), Rank-5 accuracy (R_5), and Rank-10 accuracy (R_{10}) as performance metrics [25]. R_1 , R_5 , and R_{10} are computed as the ratios of probe sequences matching the gallery sequences with correct identities when the candidate gallery sequences are the top 1, top 1 to 5, and top 1 to 10 most similar sequences to the probe sequence. Mean Average Precision (mAP) [73] is also used to quantitatively evaluate the overall performance of our approach.

4.4 Empirical Evaluation

We compare our *unsupervised* approach with state-of-the-art unsupervised skeleton-based person re-ID methods on BIWI, IAS, KGBD, and KS20 datasets, as shown in Tables 2 and 3. The latest self-supervised, supervised skeleton-based person re-ID methods [20, 23, 24] and representative hand-crafted person re-ID methods [16, 19] are also included to provide a comprehensive comparison. It should be noted that the hand-crafted methods directly extract skeleton descriptors from raw skeleton data to perform person re-ID.

4.4.1 Comparison with Self-Supervised and Unsupervised State-of-the-Art Methods

The proposed approach shows significant performance improvements over existing self-supervised and unsupervised methods on different datasets. Compared with AGE [21] and SGELA [22] that

Table 2 Performance comparison with state-of-the-art skeleton-based methods on BIWI-S, BIWI-W, and IAS-A. \ddagger indicates employing supervised fine-tuning and **Bold** denotes the best cases among self-supervised/unsupervised methods. The underline represents the highest results among all methods.

Types	Methods	BIWI-S				BIWI-W				IAS-A			
		R ₁	R ₅	R ₁₀	mAP	R ₁	R ₅	R ₁₀	mAP	R ₁	R ₅	R ₁₀	mAP
Hand-crafted	DPG [20]	18.5	45.4	63.8	6.7	6.5	15.5	20.3	8.7	16.4	39.5	53.4	11.0
	D ₁₃ [16]	28.3	53.1	65.9	13.1	14.2	20.6	23.7	17.2	40.0	58.7	67.6	24.5
	D ₁₆ [19]	32.6	55.7	68.3	16.7	17.0	25.3	29.6	18.8	42.7	62.9	70.7	25.2
Supervised	PoseGait [20]	14.0	40.7	56.7	9.9	8.8	23.0	31.2	11.1	28.4	55.7	69.2	17.5
	\ddagger SGELA [22]	29.2	65.2	73.8	<u>23.5</u>	13.9	15.3	16.7	<u>22.9</u>	18.0	32.1	46.2	13.5
	MG-SCR [23]	20.1	46.9	64.1	7.6	10.8	20.3	29.4	11.9	36.4	59.6	69.5	14.1
	\ddagger SM-SGE [24]	34.8	60.6	71.5	12.8	16.7	31.0	40.2	18.7	38.5	63.2	73.9	15.0
Self-supervised /Unsupervised	AGE [21]	25.1	43.1	61.6	8.9	11.7	21.4	27.3	12.6	31.1	54.8	67.4	13.4
	SGELA [22]	25.8	51.8	64.4	<u>15.1</u>	11.7	14.0	14.7	19.0	16.7	30.2	44.0	13.2
	SM-SGE [24]	31.3	56.3	69.1	10.1	13.2	25.8	33.5	15.2	34.0	60.5	71.6	13.6
	SimMC [25]	41.7	66.6	76.8	12.3	24.5	36.7	44.5	19.9	44.8	65.3	72.9	18.7
	Hi-MPC ^h (Ours)	<u>47.5</u>	70.3	78.6	17.4	27.3	40.3	48.8	22.6	45.6	67.3	75.4	23.2

Table 3 Performance comparison with state-of-the-art skeleton-based methods on IAS-B, KGBD, and KS20. \ddagger indicates employing supervised fine-tuning and **Bold** denotes the best cases among self-supervised/unsupervised methods. The underline represents the highest results among all methods.

Types	Methods	IAS-B				KGBD				KS20			
		R ₁	R ₅	R ₁₀	mAP	R ₁	R ₅	R ₁₀	mAP	R ₁	R ₅	R ₁₀	mAP
Hand-crafted	DPG [20]	16.0	41.2	57.3	10.6	30.0	49.1	58.1	2.1	35.2	61.5	70.5	11.3
	D ₁₃ [16]	43.7	68.6	76.7	23.7	17.0	34.4	44.2	1.9	39.4	71.7	81.7	18.9
	D ₁₆ [19]	44.5	69.1	<u>80.2</u>	24.5	31.2	50.9	59.8	4.0	51.7	77.1	86.9	<u>24.0</u>
Supervised	PoseGait [20]	28.9	51.6	62.9	20.8	50.6	67.0	72.6	<u>13.9</u>	49.4	80.9	<u>90.2</u>	23.5
	\ddagger SGELA [22]	23.6	42.9	51.9	14.8	43.7	58.7	65.0	7.1	49.7	67.0	77.1	22.2
	MG-SCR [23]	32.4	56.5	69.4	12.9	44.0	58.7	64.6	6.9	46.3	75.4	84.0	10.4
	\ddagger SM-SGE [24]	44.3	68.2	77.5	14.9	43.2	58.6	64.6	7.5	49.8	78.1	85.2	11.7
Self-supervised /Unsupervised	AGE [21]	31.1	52.3	64.2	12.8	2.9	5.6	7.5	0.9	43.2	70.1	80.0	8.9
	SGELA [22]	22.2	40.8	50.2	14.0	38.1	53.5	60.0	4.5	45.0	65.0	75.1	21.2
	SM-SGE [24]	38.9	64.1	75.8	13.3	38.2	54.2	60.7	4.4	45.9	71.9	81.2	9.5
	SimMC [25]	46.3	68.1	77.0	22.9	54.9	66.2	70.6	<u>11.7</u>	66.4	80.7	87.0	22.3
	Hi-MPC ^h (Ours)	48.2	70.2	77.8	25.3	56.9	70.2	75.1	10.2	69.6	83.5	87.1	22.0

learn skeleton features from only joint-level representations, our approach achieves higher person re-ID performance on all datasets with an improvement of 14.5-54.0% for Rank-1 accuracy, 12.5-64.6% for Rank-5 accuracy, 7.1-67.6% for Rank-10 accuracy, and 0.8-13.1% for mAP. These improvements indicate that the proposed approach can capture more discriminative features from multiple skeleton levels for person re-ID. By mining key skeletons and exploiting more informative patterns of different levels with the proposed HSM mechanism, our approach significantly outperforms the SM-SGE framework [24] that directly combines four-scale skeletons by 9.3-23.7% for Rank-1 accuracy and 5.8-12.5% for mAP on different datasets. Note that we follow [22, 25] to report the average performance of all methods for a fair comparison while there exist slight performance variations in practice. In this context, the proposed approach is still superior to the latest skeleton contrastive learning framework SimMC [25] in most cases, as shown in Tables 2 and 3.

Although SimMC obtains slightly higher mAP on KS20 and KGBD, our approach can achieve better overall performance in terms of Rank-1, Rank-5, Rank-10, and mAP on the datasets that contain frequent changes of appearances or scenes (BIWI-S, BIWI-W, IAS-A, IAS-B). Considering that these changes could induce more random perturbations or noises in the collection of skeletons, the results suggest that our approach is more robust than SimMC for learning effective skeleton representations under different conditions. Moreover, our approach is more efficient than most skeleton-based person re-ID methods in terms of the model size and computational complexity (see Appendix II).

Our approach is also evaluated on the cross-view person re-ID scenarios of KS20. As presented in Table 4, the proposed Hi-MPC^h outperforms state-of-the-art self-supervised and unsupervised counterparts by an average margin of 6.4 to 44.4% for Rank-1 accuracy and 3.0 to 48.7% for

Table 4 Cross-view person re-ID performance comparison with state-of-the-art self-supervised and unsupervised methods with CVE setup of KS20. 0° , 30° , 90° , 130° , and 180° denote different views of probe or gallery sets.

Probe Views	Gallery Views			0°			30°			90°			130°			180°					
	R_1	R_5	R_{10}	mAP	R_1	R_5	R_{10}	mAP	R_1	R_5	R_{10}	mAP	R_1	R_5	R_{10}	mAP	R_1	R_5	R_{10}	mAP	
0°	AGE [21]	46.7	74.2	83.5	22.5	11.0	35.7	47.5	10.0	8.1	29.9	47.5	9.2	7.5	26.7	43.5	8.4	7.0	23.0	37.4	8.2
	SGELA [22]	76.2	89.6	92.8	37.1	15.1	27.3	35.1	19.9	10.1	27.5	40.9	18.2	10.7	21.5	29.3	18.0	15.4	25.8	38.0	12.6
	SM-SGE [24]	58.4	84.7	92.2	27.7	17.2	50.0	63.3	10.8	7.2	21.9	39.1	10.5	4.4	19.4	34.7	9.3	10.0	23.8	33.1	9.4
	SimMC [25]	84.4	97.3	99.2	61.2	37.9	59.4	67.6	24.8	28.9	50.8	62.9	27.1	23.3	43.0	52.9	20.3	15.2	29.3	45.7	14.5
	Hi-MPC ^h (Ours)	92.2	98.4	99.6	66.9	35.6	61.7	72.7	27.3	36.7	58.6	73.1	25.9	24.6	41.8	53.5	16.4	17.2	30.1	43.8	13.2
30°	AGE	10.1	42.8	57.8	8.8	52.3	82.7	91.5	25.0	15.0	35.6	58.5	8.8	10.1	24.2	41.8	8.1	7.8	24.2	34.3	8.3
	SGELA	13.1	19.6	22.6	19.4	70.9	88.2	91.8	40.5	11.8	24.5	36.3	16.5	6.9	22.6	31.7	15.4	9.2	15.4	22.9	13.9
	SM-SGE	18.1	48.4	65.0	11.5	60.2	82.0	89.8	28.2	12.5	27.2	35.3	10.7	7.5	23.4	33.8	10.6	8.8	27.2	39.1	10.5
	SimMC	30.8	66.2	74.6	20.7	91.8	97.4	98.2	67.8	36.8	55.1	67.6	29.9	16.4	30.5	40.2	20.4	16.2	36.7	56.6	12.7
	Hi-MPC ^h (Ours)	33.2	66.4	75.8	24.4	93.8	97.7	98.8	66.5	37.5	62.1	71.5	25.1	19.5	34.8	50.0	17.8	16.8	37.5	47.7	14.3
90°	AGE	7.5	27.3	43.2	8.7	9.0	28.5	44.1	9.3	57.4	81.4	90.7	19.2	13.8	41.1	57.1	9.0	7.8	30.0	46.0	8.3
	SGELA	9.6	19.8	29.7	16.4	10.8	15.6	20.4	17.5	48.4	75.7	86.5	31.6	17.1	35.7	43.0	22.0	13.5	23.4	31.8	21.3
	SM-SGE	19.1	33.1	48.1	12.4	23.1	40.6	57.4	11.5	72.2	89.1	92.8	24.9	20.9	48.4	69.4	12.8	19.4	36.9	51.6	11.3
	SimMC	26.2	44.9	50.8	11.9	41.4	64.1	75.4	27.3	96.7	100	100	73.1	60.9	81.6	88.7	45.0	25.8	48.4	64.5	15.4
	Hi-MPC ^h (Ours)	26.2	47.7	62.1	23.0	50.8	71.5	83.2	34.0	97.3	100	100	73.9	61.7	80.5	84.8	42.2	33.2	65.2	80.1	23.1
130°	AGE	6.7	21.3	34.7	8.2	7.9	23.4	38.9	8.9	15.2	35.9	54.4	9.2	45.3	70.5	82.1	18.7	11.3	37.1	50.2	8.9
	SGELA	5.8	18.8	28.0	14.2	11.6	15.5	20.7	16.8	17.6	47.1	53.2	24.5	59.6	81.5	89.1	36.8	17.0	29.8	32.5	23.0
	SM-SGE	8.4	24.4	37.8	10.4	12.9	26.6	36.3	10.9	24.1	53.4	66.3	12.9	64.4	85.9	95.0	25.5	17.8	40.9	59.1	12.1
	SimMC	18.0	32.4	48.8	14.2	24.2	44.9	59.4	15.7	60.2	78.1	86.7	45.2	92.5	98.8	99.2	71.5	30.1	55.1	66.8	18.8
	Hi-MPC ^h (Ours)	19.9	39.1	55.1	20.3	20.7	50.8	68.4	21.9	62.1	80.5	87.5	45.8	93.4	99.2	99.2	72.8	36.3	61.3	75.8	26.3
180°	AGE	7.9	17.7	32.6	8.1	5.2	22.4	33.4	8.3	10.5	25.6	34.0	8.2	11.6	33.1	52.9	8.8	47.1	72.4	82.6	22.6
	SGELA	14.0	29.1	39.2	21.3	11.9	20.6	25.9	17.3	18.6	37.8	49.7	19.4	22.7	45.9	55.2	20.7	74.5	92.7	95.1	38.3
	SM-SGE	5.6	20.0	30.6	8.5	6.6	22.7	31.6	8.6	13.8	34.1	45.6	9.4	10.3	37.5	56.6	10.4	51.9	79.7	87.8	25.6
	SimMC	19.1	39.5	48.8	15.3	14.1	28.1	40.6	14.0	25.8	44.1	53.5	29.8	36.9	61.3	74.6	32.0	91.0	97.7	98.4	59.5
	Hi-MPC ^h (Ours)	16.8	34.4	47.6	15.6	14.8	30.9	44.5	14.8	30.9	55.5	68.0	25.8	37.1	62.5	79.3	29.5	93.0	97.3	98.8	58.0

mAP on all views, and also surpasses the latest SimMC framework [25] in most probe-gallery matching views. This suggests that our model is more effective on learning generalized (*i.e.*, view-independent) skeleton representations with higher robustness to viewpoint changes for cross-view person re-ID.

4.4.2 Comparison with Hand-Crafted and Supervised State-of-the-Art Methods

The results in Tables 2 and 3 show that our model achieves better person re-ID performance than the representative hand-crafted methods D_{13} [16] and D_{16} [19] that utilize numerous anthropometric skeleton descriptors by 3.7-39.9% for Rank-1 accuracy and 0.7-8.3% for mAP on four of the six testing sets (BIWI-S, BIWI-W, IAS-B, KGBD). Although they achieve competitive mAP on datasets with frequent appearance and viewpoint changes (IAS-A, KS20), our approach can obtain higher overall performance in terms of Rank-1 accuracy (2.9-30.2%), Rank-5 accuracy (4.4-11.8%), and Rank-10 accuracy (0.2-7.8%). Notably, the proposed unsupervised approach markedly outperforms supervised state-of-the-art models PoseGait [20] and MG-SCR [23] on almost all datasets. Interestingly, with extra labels to

fine-tune SGELA [22] and SM-SGE [24], those methods still perform poorly on many datasets. In contrast, our approach achieves better and more stable performance on all datasets without using any skeletal annotation. This shows that Hi-MPC^h has good generality with greater potential for use in practical person re-ID scenarios.

5 Further Analysis

5.1 Evaluation on RGB-Estimated Skeleton Data

In this section, we verify the generality of our skeleton-based approach under the large-scale RGB scenarios (CASIA-B). We leverage pre-trained pose estimation models [78, 79] to extract 3D skeleton data from RGB videos of CASIA-B, and evaluate the performance of our approach with the estimated skeleton data. As shown in Table 5, we compare our model with state-of-the-art skeleton-based methods [21, 22, 24, 25] and representative appearance-based methods [72, 74–77]. Our approach achieves superior performance to most state-of-the-art skeleton-based methods (AGE [21], SM-SGE [24], SGELA [22]) with a significant margin of 11.3 to 64.7% for Rank-1 accuracy and 0.2 to 7.7% for mAP in different evaluation conditions of CASIA-B. Compared

Table 5 Performance comparison with appearance-based and skeleton-based methods on CASIA-B. “Clothes-Normal” represents the probe set under “Clothes” condition and gallery set under “Normal” condition. ♣ refers to appearance-based methods and ‡ represents requiring label information for training. “—” indicates no published result.

Probe-Gallery	Normal-Normal				Bags-Bags				Clothes-Clothes				Clothes-Normal				Bags-Normal			
	R ₁	R ₅	R ₁₀	mAP	R ₁	R ₅	R ₁₀	mAP	R ₁	R ₅	R ₁₀	mAP	R ₁	R ₅	R ₁₀	mAP	R ₁	R ₅	R ₁₀	mAP
‡LMNN♣ [74]	3.9	22.7	36.1	—	18.3	38.6	49.2	—	17.4	35.7	45.8	—	11.6	12.6	17.8	—	23.1	37.1	44.4	—
‡ITML♣ [75]	7.5	22.2	34.2	—	19.5	26.0	33.7	—	20.1	34.4	43.3	—	10.3	24.5	36.1	—	21.8	30.4	36.3	—
‡ELF♣ [76]	12.3	35.6	50.3	—	5.8	25.5	37.6	—	19.9	43.9	56.7	—	5.6	16.0	26.3	—	17.1	30.0	37.9	—
SDALF♣ [77]	4.9	27.0	41.6	—	10.2	33.5	47.2	—	16.7	42.0	56.7	—	11.6	19.4	27.6	—	22.9	30.1	36.1	—
‡Score-based MLR♣ [72]	13.6	48.7	63.7	—	13.6	48.7	63.7	—	13.5	48.6	63.9	—	9.7	27.8	45.1	—	14.7	32.6	50.2	—
‡Feature-based MLR♣ [72]	16.3	43.4	60.8	—	18.9	44.8	59.4	—	25.4	53.3	68.9	—	20.3	42.6	56.9	—	31.8	53.6	64.1	—
AGE [21]	20.8	29.3	34.2	3.5	37.1	56.2	67.0	9.8	35.5	54.3	65.3	9.6	14.6	33.0	42.7	3.0	32.4	51.2	60.1	3.9
SM-SGE [24]	50.2	73.5	81.9	6.6	26.6	49.0	59.4	9.3	27.2	51.4	63.2	9.7	10.6	26.3	35.9	3.0	16.6	36.8	47.5	3.5
SGELA [22]	71.8	87.5	91.4	9.8	48.1	69.5	77.7	16.5	51.2	73.8	81.5	7.1	15.9	30.8	40.6	4.7	36.4	57.1	64.6	6.7
SimMC [25]	80.8	92.3	93.7	10.8	69.1	86.6	91.3	16.5	68.0	88.1	93.0	15.7	25.6	43.8	54.0	5.4	42.0	59.8	68.9	7.1
Hi-MPC ^h (Ours)	85.5	94.9	95.8	11.2	71.2	87.5	92.1	17.0	70.2	88.5	92.6	14.1	27.2	45.0	54.9	4.9	50.1	65.5	72.1	7.5

Table 6 Ablation study with different configurations: Direct prototype contrastive learning (DPC), meta-prototype contrastive learning (MPC), and hard skeleton mining mechanism (HSM). “Hi” denotes adopting hierarchical skeleton representations (*i.e.*, combining skeleton-level, component-level and limb-level representations) and exploiting the proposed MSMR for person re-ID. The configurations (ID = 1, 2, 3, 5) without using “Hi” adopt the original skeleton representation (*i.e.*, joint-level representations). “+” indicates using the corresponding component.

ID	Configurations	BIWI-S		BIWI-W		IAS-A		IAS-B		KGBD		KS20	
		R ₁	mAP										
1	Baseline	24.8	9.3	10.9	14.1	29.4	13.8	30.2	13.3	20.5	4.4	17.0	9.5
2	+ DPC	38.3	10.7	19.9	19.7	35.4	16.3	35.4	16.6	53.7	8.5	63.3	17.6
3	+ MPC	39.8	13.1	22.4	19.3	38.4	17.0	37.3	14.4	53.2	8.1	63.9	18.5
4	+ Hi + MPC	40.4	12.8	24.2	21.1	42.2	19.4	38.2	18.9	55.3	8.7	66.4	18.6
5	+ MPC + HSM	44.9	14.2	23.7	21.0	40.0	17.8	42.8	23.1	55.8	9.5	66.2	19.0
6	+ Hi + MPC + HSM	47.5	17.4	27.3	22.6	45.6	23.2	48.2	25.3	56.9	10.2	69.6	22.0

with the latest contrastive learning framework SimMC [25], our model performs better in most conditions, which justifies its effectiveness on learning more discriminative skeleton representations when applied to RGB-estimated skeleton data. Our skeleton-based approach also achieves higher results than several representative classical appearance-based methods that employ visual metric learning with RGB-based appearances and textures (LMNN [74], ITML [75], ELF [76], SDALF [77]) or leverage both gait energy images and appearance features (MLR [72]) on different conditions. It should be noted that directly comparing skeleton-based method with appearance-based methods might be unfair as they use different learning manners (*e.g.*, supervised or unsupervised learning) and fundamentally different data modalities (*e.g.*, gait energy images). However, these classic representative methods can serve as a baseline performance reference under the same evaluation protocol [25, 72]. The highly competitive performance of the proposed approach on RGB-estimated skeletons demonstrates its generality and value for person re-ID under large-scale RGB-based scenarios.

5.2 Ablation Study

We conduct ablation study to demonstrate the contribution of each component in our approach. The raw skeleton sequences, *i.e.*, concatenation of 3D coordinates of body joints, are adopted as the baseline for comparison. As reported in Table 6, employing direct skeleton prototype contrastive (DPC) learning (ID = 2) significantly improves the person re-ID performance of the baseline especially on more challenging datasets such as KGBD (up to 33.2% for Rank-1 accuracy) and KS20 (up to 46.3% for Rank-1 accuracy). This suggests that prototypes are indeed more representative skeleton features than raw 3D skeletons and DPC plays a crucial role in exploiting such discriminative features from different individuals. The proposed meta-prototype contrastive (MPC) learning (ID = 3) performs better than DPC (ID = 2) in almost all cases when applied to joint-level skeleton representations. Combining hierarchical skeleton representations for multi-level clustering and meta-prototype contrastive learning (ID = 4) achieves better performance than joint-level DPC (ID = 2) by up to 6.8% for Rank-1 accuracy and 3.1% for mAP on different datasets.

Table 7 Performance of our approach on different datasets when solely exploiting limb-level (L), component-level (C), joint-level skeleton representations (J) or MSMR that combines all level skeleton representations for person re-ID. We compare our approach and the naive Hi-MPC without using HSM. “✓” indicates using the corresponding configurations.

ID	L	C	J	HSM	BIWI-S		BIWI-W		IAS-A		IAS-B		KGBD		KS20	
					R ₁	mAP										
1	✓				35.7	12.1	18.0	16.8	35.2	16.1	38.0	18.3	42.5	5.5	59.2	15.6
2		✓			38.9	12.2	21.8	18.1	36.9	16.0	38.0	19.8	50.0	7.0	59.8	16.4
3			✓		39.3	12.3	22.4	19.3	38.4	17.0	37.3	14.4	51.5	7.7	61.8	16.5
4	✓	✓	✓		40.4	12.8	24.2	21.1	42.2	19.4	38.2	18.9	55.3	8.7	65.4	18.2
5	✓			✓	36.9	12.4	17.5	16.3	35.5	17.7	40.1	19.3	44.3	5.7	64.1	17.9
6		✓		✓	41.8	15.1	22.3	18.9	41.7	18.1	44.6	20.5	52.3	7.9	66.0	18.8
7			✓	✓	44.9	14.2	23.7	21.0	40.0	17.8	41.7	20.1	55.8	9.5	65.4	18.9
8	✓	✓	✓	✓	47.5	17.4	27.3	22.6	45.6	23.2	48.2	25.3	56.9	10.2	69.6	22.0

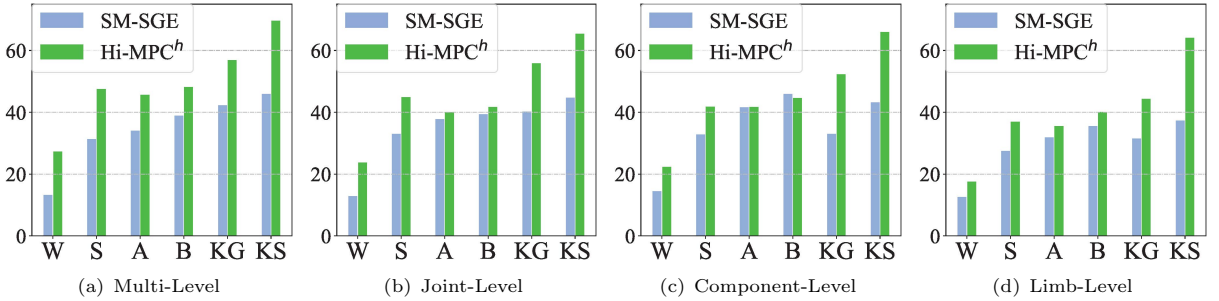


Fig. 5 Performance (Rank-1 accuracy) of our approach with different level representations (joint-level, component-level, limb-level) and their combination (multi-level) on BIWI-W (W), BIWI-S (S), IAS-A (A), IAS-B (B), KGBD (KG), and KS20 (KS) testing sets. The latest multi-level method SM-SGE [24] is compared under the same setting of skeleton levels.

Such results verify the effectiveness of the proposed Hi-MPC, as it can capture richer body and motion patterns via exploiting the most typical skeleton features from various levels. The effects of different level skeleton representations will be also discussed in Sec. 5.3. The proposed approach (Hi-MPC^h) employing the hard skeleton mining (HSM) mechanism (ID = 6) achieves consistent performance improvement of 1.6-10.0% for Rank-1 accuracy and 1.2-6.4% for mAP compared with naïve Hi-MPC (ID = 4) on all datasets. Adding HSM (ID = 5) also improves the performance of MPC (ID = 3), which suggests the general validity of HSM for both single-level and hierarchical skeleton contrastive learning. These results further suggest that HSM can facilitate mining key skeletons to learn highly informative and valuable skeletal patterns during skeleton meta-prototype contrastive learning for person re-ID. Further visualization and analysis of the HSM mechanism are provided in Sec. 5.5.

5.3 Evaluation on Different Level Skeleton Representations

We evaluate the performance of limb-level, component-level, joint-level skeleton representations and their combination in the proposed approach. As shown in Table 7, different level skeleton representations (ID = 5-7) learned by our final approach can *individually* achieve highly competitive performance on different datasets, which suggests the great potential of higher level skeleton representations such as key limbs to be directly applied for person re-ID. Notably, the model exploiting joint-level (ID = 3, 7) and component-level skeleton representations (ID = 2, 6) achieves higher performance than using limb-level (ID = 1, 5) in most cases. This demonstrates the greater contribution of low-level skeleton representations, as they usually contain more specific positional and structural information of body parts than high-level ones to benefit learning more discriminative features for person re-ID. Furthermore, combining hierarchical skeleton representations of all levels (ID = 4, 8) attains the best person re-ID performance on different

Table 8 Performance of our approach with different meta-transformation heads ($M = 1, 4, 8, 16$).

M	BIWI-S		BIWI-W		IAS-A		IAS-B		KS20		KGBD	
	R ₁	mAP										
1	45.7	15.3	25.7	22.5	43.8	21.1	46.7	25.0	67.2	20.6	55.5	9.2
4	47.1	17.6	26.6	22.9	45.0	22.5	48.1	26.8	69.2	21.3	56.5	10.0
8	47.5	17.4	27.3	22.6	45.6	23.2	48.2	25.3	69.6	22.0	56.9	10.2
16	48.5	16.9	27.7	23.9	46.0	24.0	48.2	25.4	70.7	21.4	57.0	9.7

Table 9 Performance of our approach with different embedding sizes ($h = 64, 128, 256, 512$).

h	BIWI-S		BIWI-W		IAS-A		IAS-B		KS20		KGBD	
	R ₁	mAP										
64	45.1	16.3	25.1	21.6	44.0	21.7	46.5	24.5	69.2	21.4	54.7	8.7
128	47.0	17.5	27.5	22.9	45.0	22.9	49.3	26.9	69.7	20.8	55.1	9.5
256	47.5	17.4	27.3	22.6	45.6	23.2	48.2	25.3	69.6	22.0	56.9	10.2
512	47.0	15.7	26.2	22.3	42.5	21.8	49.5	27.3	70.7	22.0	55.8	9.2

datasets when compared to single-level representations (ID = 1-3, 5-7), regardless of using HSM. Such results further verify the necessity of the proposed hierarchical skeleton representations, as the multi-level skeletal modeling can encourage mining more unique body and motion features for person re-ID, which is consistent with the analysis in [23, 24].

We also compare the performance of different-level skeleton representations learned by our approach with the latest multi-level graph framework SM-SGE [24]. As presented in Fig. 5, our approach not only significantly outperforms SM-SGE using multi-level representations, but also gains superior performance when applying the learned higher level representations for person re-ID on five of six testing sets. This further demonstrates the effectiveness of our approach on learning more useful skeleton features at various levels. It is interesting to observe that the component-level representations with a simpler body structure can perform comparably or even better than joint-level representations on half of datasets. This implies that the original skeletons of those datasets might contain redundant positional or structural information, which can be compressed and characterized with more concise and abstract skeleton representations to better achieve person re-ID.

5.4 Discussions

5.4.1 Effects of Meta-Transformation Heads

Table 8 presents the effects of different numbers of meta-transformation heads. Employing more learnable meta-transformation heads is shown to

improve the performance of our approach on different datasets, which demonstrates the effectiveness of exploiting different contrastive subspaces for better skeleton representation learning. It is worth noting that the model performance tends to be stable when applying many more heads, as it could introduce more random perturbation into contrastive learning and help obtain more robust prototype estimation (see Sec. 3.2). More analysis is provided in the Appendices.

5.4.2 Effects of Embedding Sizes

As shown in Table 9, our approach achieves higher performance with relatively larger embedding sizes ($h \geq 128$) on all datasets. The results suggest that a small embedding size ($h = 64$) could be insufficient to learn effective skeleton representations for person re-ID, while using too large sizes of embedding (*e.g.*, $h = 512$) might cause the model to learn more redundant feature information and degrade the overall performance.

5.4.3 Different Settings of DBSCAN

We evaluate the effects of the two main parameters in the DBSCAN algorithm, *i.e.*, minimum sample amount a_{min} within the maximum distance ϵ , which are empirically selected to encourage more balanced and stable clustering. As presented in Table 10, a_{min} seems to have no significant effect on the performance of our approach, as setting different values of a_{min} achieve similar accuracy on most datasets. Nevertheless, it is worth mentioning that employing too small a value for a_{min} tends to generate much larger clusters and might

Table 10 Performance of our approach when setting different minimum sample amount ($a_{min} = 1, 2, 3, 4$) for DBSCAN.

a_{min}	BIWI-S		BIWI-W		IAS-A		IAS-B		KS20		KGDB	
	R ₁	mAP										
1	46.6	17.6	26.6	21.0	44.7	22.1	48.5	26.1	68.4	21.1	54.7	9.6
2	47.5	17.4	27.3	22.6	45.6	23.2	48.2	25.3	69.6	22.0	56.3	10.0
3	48.8	18.1	27.7	23.2	44.8	22.7	49.0	25.7	70.3	21.7	56.9	10.2
4	46.9	17.8	27.6	23.3	45.4	23.2	49.1	26.1	69.0	20.8	56.3	10.2

Table 11 Performance of our approach when setting different maximum distances ($\epsilon = 0.4, 0.6, 0.8, 1.0$) for DBSCAN.

ϵ	BIWI-S		BIWI-W		IAS-A		IAS-B		KS20		KGDB	
	R ₁	mAP										
0.4	46.8	16.6	19.9	18.7	43.2	18.2	42.0	20.0	69.5	20.7	55.6	7.8
0.6	47.5	17.4	22.4	19.2	44.7	20.7	46.7	25.8	69.4	21.8	56.9	10.2
0.8	50.3	18.2	27.3	22.6	45.6	23.2	48.2	25.3	69.6	22.0	47.9	4.8
1.0	27.9	9.7	11.6	14.2	33.8	13.6	37.2	14.3	50.0	11.0	46.9	4.3

lead to a degeneration of clustering (*e.g.*, single super cluster) and unstable model training in practice.

Large values of ϵ (*e.g.*, $\epsilon = 1.0$) greatly reduce the performance of our approach, as shown in Table 11. Considering that larger ϵ leads to higher connectedness of instances, *i.e.*, larger cluster and smaller number of prototypes, the results demonstrate that setting a relatively lower ϵ value with more diverse skeleton prototypes could facilitate learning richer discriminative features for person re-ID. However, too small a value for ϵ could cause excessive over-clustering, which leads to the degradation of model performance on some datasets.

5.4.4 Effects of Sequence Lengths

We evaluate multi-shot performance of our approach with different settings of sequence lengths F (*i.e.*, F -shot person re-ID), and compare it with the latest SimMC [25] on different datasets. As shown in Fig. 6, the proposed Hi-MPC^h consistently outperforms SimMC on all cases of datasets and sequence lengths. In contrast to SimMC that fails to keep high accuracy when F varies slightly, our approach is more stable with better results on different datasets. Since skeleton sequences contain more pattern features as F increases, our approach is capable of learning more effective skeleton representations to achieve larger performance improvement in most cases. Nevertheless, it is interesting to note that using shorter sequences sometimes performs better than longer sequences on small datasets such as IAS-B, implying that a larger size of available training

sequences under smaller F settings could help learn better representations on those datasets.

5.5 Analysis of Hard Skeleton Mining

To verify the effectiveness of the proposed HSM mechanism on mining more informative skeletons, we visualize joint-level, component-level, and limb-level skeleton representations with their inferred importance on different datasets. As shown in Fig. 7, the higher importance is often assigned to either evidently different skeletons or dramatically changing poses in the sequence, which could introduce more pattern information compared with other similar skeletons. This is consistent with our intuition that skeletons containing diverse patterns (*i.e.*, higher intra-class variation) are harder to be recognized as the same person, thus deserving more attention to learn during training. It is also observed that there exists a good alignment of informative importance between component-level and limb-level skeleton representations, while our model focuses on more key skeletons with continuous patterns at joint-level, which suggests that the proposed approach may hierarchically capture different skeleton semantics (*e.g.*, pattern consistency) to mine more effective features from various levels.

The proposed HSM mechanism allows us to intuitively visualize the importance/value of each skeleton in learning *hard* patterns and useful features. As shown in Fig. 7, the component-level skeleton representations with a simpler body structure are highly similar with the joint-level skeleton representations to effectively characterize

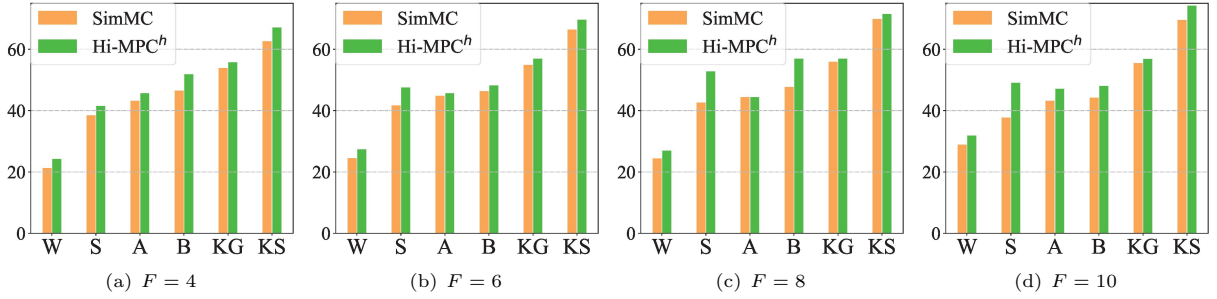


Fig. 6 Multi-shot person re-ID performance (Rank-1 accuracy) of our approach with different settings of sequence lengths ($F = 4, 6, 8, 10$) on BIWI-W (W), BIWI-S (S), IAS-A (A), IAS-B (B), KGBD (KG), and KS20 (KS) testing sets. The latest state-of-the-art method SimMC [25] is compared as the performance baseline.

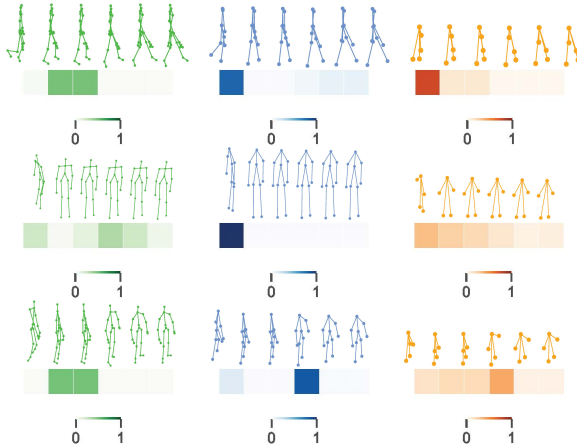


Fig. 7 Visualization of joint-level (green), component-level (blue), limb-level representations (orange) of consecutive skeletons and their informative importance in different datasets. Each row shows three level representations of the same sequence. Darker colors of i^{th} position in heat maps indicate higher importance of i^{th} skeleton representation.

body poses, while the limb-level ones can provide more global motion dynamics of skeletons. This further suggests the potential of more concise and abstract skeleton representations on learning unique patterns for person re-ID. Moreover, as hard skeletons typically contain easily-confused or uncommon patterns, we can potentially exploit hard skeleton mining to detect special skeletons/poses (e.g., abnormal or pathological gaits) of a certain person for more advanced tasks such as medical gait analysis. It could also be used to discover noisy skeletons with incomplete or extremely unnatural poses for efficient skeleton filtration and selection.

5.6 t-SNE Visualization of Skeleton Representations

We provide a qualitative analysis with t-SNE [80] visualization of skeleton representations, which are compared with two skeleton-based state-of-the-art methods, SM-SGE [24] and SimMC [25]. As shown in Fig. 8(c), the proposed MSMR learned from our approach achieves higher inter-identity separation than representations learned from SM-SGE. Compared with SimMC, our method is able to simultaneously learn coarse-to-fine (e.g., joint-level, component-level) skeleton representations with lower entropy, which forms evident identity groups in different levels, as shown in Fig. 8(d) and 8(e). Such results not only suggest the effectiveness of Hi-MPC^h on learning discriminative representations (i.e., differences between ground-truth classes) from *unlabeled* 3D skeleton data, but also demonstrate its ability on learning skeleton semantics (e.g., identity-specific patterns) at different levels, which is consistent with the conclusions in Sec. 5.3. However, it can be that the limb-level skeleton representations with the much more abstract body structure are more difficult to be clustered in the t-SNE visualization (see Fig. 8(f)). This implies that too much information loss of skeleton positions, structures, and dynamics (e.g., full dynamics of all joints) could reduce the model performance on learning recognizable pattern information of different identities.

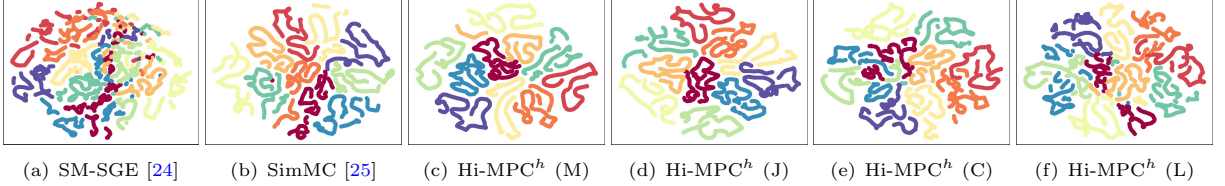


Fig. 8 t-SNE visualization of skeleton representations learned from SM-SGE (a), SimMC (b), and Hi-MPC^h ((c)-(f)) for the first 10 identities in BIWI. We visualize MSMR (M), joint-level (J), component-level (C), and limb-level representations (L) learned by Hi-MPC^h in (c), (d), (e), and (f), respectively. Features of different identities are shown in different colors.

6 Conclusion and Future Work

In this paper, we proposed a hierarchical skeleton meta-prototype contrastive learning (Hi-MPC) approach with a hard skeleton mining (HSM) mechanism to contrast and learn the most representative features from key informative skeletons for unsupervised person re-ID. The hierarchical representations of 3D skeletons are built to capture coarse-to-fine body features from different levels. To encourage more consistent contrastive learning to mine more representative skeleton prototypes, we propose to perform meta-transformation of instances and prototypes to contrast in multiple contrastive feature subspaces. We further devise a hard skeleton mining mechanism to assign larger importance to harder skeletons, so as to learn more valuable patterns and effective representations. Finally, we combine different level skeleton features learned from our approach to construct multi-level skeleton meta-representation (MSMR) for person re-ID. Our approach outperforms most state-of-the-art methods, and is also highly effective when applied to multi-view and RGB-based scenarios with estimated skeletons.

Applicability. Our model can be applied to either sensor-based skeleton data or RGB-estimated skeleton data. On the one hand, our approach can perform person re-ID using *unlabeled* 3D skeleton data *directly* captured from depth sensors such as Kinect. The quality of sensor-based skeleton data mainly depends on the precision of sensor algorithm (*e.g.*, skeleton estimation algorithm of Kinect [14]) and capture distance (*i.e.*, physical distance between sensor and subject). These factors influence the noise existed in the skeleton data and thus affect the performance of our model. On the other hand, when there are only cameras or images available, we can exploit

state-of-the-art pose estimation models to first extract skeleton data from RGB images and then apply our model for person re-ID. The quality of RGB-estimated skeleton data highly relies on the precision of pose estimation models and the quality (*e.g.*, resolution) of the original RGB images, while their noise is typically larger than sensor-based skeletons using depth information. In this sense, the performance of our model can be further improved with higher-quality estimated skeletons.

Limitation. Despite achieving highly competitive performance on existing skeleton-based person re-ID benchmarks, our study has some limitations as follows. The 3D skeletons in this work are mainly collected from prevailing depth sensors such as Kinect [14] under controllable environments, while diverse skeleton collection (*e.g.*, different devices in uncontrollable environments) should be further studied for more general person re-ID scenarios. On the other hand, the person re-ID models under open-scenario (*e.g.*, long-distance, cross-device) skeleton data are not thoroughly investigated in this work, so more advanced sensor devices are expected to help collect such skeleton data with higher quality to validate model effectiveness. Compared with existing RGB-based person re-ID datasets (*e.g.*, MSMT17), the scale of datasets used in this study is relatively limited. Considering the lack of large-scale 3D skeleton person re-ID benchmarks, we will collect and open more advanced and challenging skeleton datasets.

We believe that this work will promote the progress of general lightweight person re-ID models with 3D skeleton data, and there are several potential directions for future works. The hierarchical clustering can be further improved by aggregating key relational features among different level skeleton representations. Incorporating

self-supervised pretext tasks (*e.g.*, skeletal action prediction) into meta-prototype contrastive learning could encourage capture of more valuable skeleton semantics for downstream tasks. More fine-grained hard skeleton mining mechanisms, such as ranking harder sequences or joints, can be devised to better guide the clustering and contrastive learning. Another potential direction is to explore diverse skeleton augmentation strategies to improve the sample capacity for higher-quality prototype learning. The generality of our model allows it to be transferred to various skeleton-based tasks, and it can hopefully synergize other data modalities (*e.g.*, depth/RGB images) to drive more pattern recognition tasks. Considering the gaps existed in different data modalities and evaluation protocols (*e.g.*, probe/gallery settings, single/multi-shot recognition), we will also explore a fair cross-modality evaluation and comparison protocol for comparing skeleton-based methods and different RGB/depth-based methods or multi-modal methods in our future work.

Declarations

- Funding: This research is supported by the National Research Foundation, Singapore under its AI Singapore Programme (AISG Award No: AISG2-PhD/2022-01-034[T]).
- Conflict of interest: The authors declare they have no conflict of interest.
- Availability of data, materials, and codes: All are available at <https://github.com/Kali-Hac/Hi-MPC>.
- Ethical statements: The datasets used in our work are officially shared by reliable research agencies, which guarantee that the collecting, processing, releasing, and using of data have gained the formal consent of participants. To protect privacy, all individuals are anonymized with simple identity numbers. Our models and codes must only be used for legitimate research.

References

- [1] A. Nambiar, A. Bernardino, and J. C. Nascento, “Gait-based person re-identification: A survey,” *ACM Computing Surveys*, vol. 52, no. 2, p. 33, 2019.
- [2] W.-S. Zheng, S. Gong, and T. Xiang, “Towards open-world person re-identification by one-shot group-based verification,” *IEEE Transactions on Pattern Analysis and Machine Intelligence*, vol. 38, no. 3, pp. 591–606, 2015.
- [3] D. Baltieri, R. Vezzani, and R. Cucchiara, “Sarc3D: a new 3D body model for people tracking and re-identification,” in *International Conference on Image Analysis and Processing*. Springer, 2011, pp. 197–206.
- [4] R. Vezzani, D. Baltieri, and R. Cucchiara, “People reidentification in surveillance and forensics: A survey,” *ACM Computing Surveys*, vol. 46, no. 2, p. 29, 2013.
- [5] C. Su, F. Yang, S. Zhang, Q. Tian, L. S. Davis, and W. Gao, “Multi-task learning with low rank attribute embedding for multi-camera person re-identification,” *IEEE Transactions on Pattern Analysis and Machine Intelligence*, vol. 40, no. 5, pp. 1167–1181, 2018.
- [6] Y.-C. Chen, X. Zhu, W.-S. Zheng, and J.-H. Lai, “Person re-identification by camera correlation aware feature augmentation,” *IEEE Transactions on Pattern Analysis and Machine Intelligence*, vol. 40, no. 2, pp. 392–408, 2018.
- [7] J. Li, A. J. Ma, and P. C. Yuen, “Semi-supervised region metric learning for person re-identification,” *International Journal of Computer Vision*, vol. 126, no. 8, pp. 855–874, 2018.
- [8] M. Li, X. Zhu, and S. Gong, “Unsupervised tracklet person re-identification,” *IEEE Transactions on Pattern Analysis and Machine Intelligence*, vol. 42, no. 7, pp. 1770–1782, 2019.
- [9] X. Qian, Y. Fu, T. Xiang, Y. Jiang, and X. Xue, “Leader-based multi-scale attention deep architecture for person re-identification.” *IEEE Transactions on Pattern Analysis and Machine Intelligence*, vol. 42, no. 2, pp. 371–385, 2019.
- [10] L. Lan, X. Wang, G. Hua, T. S. Huang, and D. Tao, “Semi-online multi-people tracking by re-identification,” *International Journal of Computer Vision*, vol. 128, no. 7, pp. 1937–1955, 2020.
- [11] H.-X. Yu, A. Wu, and W.-S. Zheng, “Unsupervised person re-identification by deep asymmetric metric embedding,” *IEEE Transactions on Pattern Analysis and Machine Intelligence*

Intelligence, vol. 42, no. 4, pp. 956–973, 2020.

[12] A. Wu, W.-S. Zheng, S. Gong, and J. Lai, “RGB-IR person re-identification by cross-modality similarity preservation,” *International Journal of Computer Vision*, vol. 128, no. 6, pp. 1765–1785, 2020.

[13] M. Ye, J. Shen, G. Lin, T. Xiang, L. Shao, and S. C. Hoi, “Deep learning for person re-identification: A survey and outlook,” *IEEE Transactions on Pattern Analysis and Machine Intelligence*, vol. 44, no. 6, pp. 2872–2893, 2021.

[14] J. Shotton, A. Fitzgibbon, M. Cook, T. Sharp, M. J. Finocchio, R. Moore, A. A. Kipman, and A. Blake, “Real-time human pose recognition in parts from single depth images,” in *Proceedings of the IEEE Conference on Computer Vision and Pattern Recognition (CVPR)*, 2011, pp. 1297–1304.

[15] M. Munaro, A. Basso, A. Fossati, L. Van Gool, and E. Menegatti, “3D reconstruction of freely moving persons for re-identification with a depth sensor,” in *International Conference on Robotics and Automation (ICRA)*. IEEE, 2014, pp. 4512–4519.

[16] M. Munaro, A. Fossati, A. Basso, E. Menegatti, and L. Van Gool, “One-shot person re-identification with a consumer depth camera,” in *Person Re-Identification*. Springer, 2014, pp. 161–181.

[17] I. B. Barbosa, M. Cristani, A. Del Bue, L. Bazzani, and V. Murino, “Re-identification with RGB-D sensors,” in *the European Conference on Computer Vision (ECCV) Workshop*. Springer, 2012, pp. 433–442.

[18] V. O. Andersson and R. M. Araujo, “Person identification using anthropometric and gait data from Kinect sensor,” in *Proceedings of the AAAI Conference on Artificial Intelligence (AAAI)*, 2015, pp. 425–431.

[19] P. Pala, L. Seidenari, S. Berretti, and A. Del Bimbo, “Enhanced skeleton and face 3D data for person re-identification from depth cameras,” *Computers & Graphics*, vol. 79, pp. 69–80, 2019.

[20] R. Liao, S. Yu, W. An, and Y. Huang, “A model-based gait recognition method with body pose and human prior knowledge,” *Pattern Recognition*, vol. 98, p. 107069, 2020.

[21] H. Rao, S. Wang, X. Hu, M. Tan, H. Da, J. Cheng, and B. Hu, “Self-supervised gait encoding with locality-aware attention for person re-identification,” in *International Joint Conference on Artificial Intelligence (IJCAI)*, vol. 1, 2020, pp. 898–905.

[22] H. Rao, S. Wang, X. Hu, M. Tan, Y. Guo, J. Cheng, X. Liu, and B. Hu, “A self-supervised gait encoding approach with locality-awareness for 3D skeleton based person re-identification,” *IEEE Transactions on Pattern Analysis and Machine Intelligence*, no. 01, pp. 1–1, 2021.

[23] H. Rao, S. Xu, X. Hu, J. Cheng, and B. Hu, “Multi-level graph encoding with structural-collaborative relation learning for skeleton-based person re-identification,” in *International Joint Conference on Artificial Intelligence (IJCAI)*, 2021, pp. 973–980.

[24] H. Rao, X. Hu, J. Cheng, and B. Hu, “SMSGE: A self-supervised multi-scale skeleton graph encoding framework for person re-identification,” in *Proceedings of the 29th ACM International Conference on Multimedia*, 2021, pp. 1812–1820.

[25] H. Rao and C. Miao, “SimMC: Simple masked contrastive learning of skeleton representations for unsupervised person re-identification,” in *International Joint Conference on Artificial Intelligence (IJCAI)*, 2022, pp. 1290–1297.

[26] —, “Transg: Transformer-based skeleton graph prototype contrastive learning with structure-trajectory prompted reconstruction for person re-identification,” in *Proceedings of the IEEE Conference on Computer Vision and Pattern Recognition (CVPR)*, 2023, pp. 22118–22128.

[27] H. Rao, Y. Li, and C. Miao, “Revisiting-reciprocal distance re-ranking for skeleton-based person re-identification,” *IEEE Signal Processing Letters*, vol. 29, pp. 2103–2107, 2022.

[28] H. Rao and C. Miao, “Skeleton prototype contrastive learning with multi-level graph relation modeling for unsupervised person re-identification,” *arXiv preprint arXiv:2208.11814*, 2022.

[29] L. Wang, T. Tan, H. Ning, and W. Hu, “Silhouette analysis-based gait recognition for human identification,” *IEEE Transactions on*

Pattern Analysis and Machine Intelligence, vol. 25, no. 12, pp. 1505–1518, 2003.

[30] C. Wang, J. Zhang, L. Wang, J. Pu, and X. Yuan, “Human identification using temporal information preserving gait template,” *IEEE Transactions on Pattern Analysis and Machine Intelligence*, vol. 34, no. 11, pp. 2164–2176, 2011.

[31] T. Wang, S. Gong, X. Zhu, and S. Wang, “Person re-identification by discriminative selection in video ranking,” *IEEE Transactions on Pattern Analysis and Machine Intelligence*, vol. 38, no. 12, pp. 2501–2514, 2016.

[32] R. Zhao, W. Oyang, and X. Wang, “Person re-identification by saliency learning,” *IEEE Transactions on Pattern Analysis and Machine Intelligence*, vol. 39, no. 2, pp. 356–370, 2017.

[33] Z. Zhang, C. Lan, W. Zeng, and Z. Chen, “Densely semantically aligned person re-identification,” in *Proceedings of the IEEE Conference on Computer Vision and Pattern Recognition (CVPR)*, 2019, pp. 667–676.

[34] N. Karianakis, Z. Liu, Y. Chen, and S. Soatto, “Reinforced temporal attention and split-rate transfer for depth-based person re-identification,” in *Proceedings of the European Conference on Computer Vision (ECCV)*. Springer, 2018, pp. 715–733.

[35] Y. Ge, F. Zhu, D. Chen, R. Zhao, and H. Li, “Self-paced contrastive learning with hybrid memory for domain adaptive object Re-ID,” in *Advances in Neural Information Processing Systems (NeurIPS)*, vol. 33, 2020, pp. 11 309–11 321.

[36] F. Han, B. Reily, W. Hoff, and H. Zhang, “Space-time representation of people based on 3D skeletal data: A review,” *Computer Vision and Image Understanding*, vol. 158, pp. 85–105, 2017.

[37] J.-H. Yoo, M. S. Nixon, and C. J. Harris, “Extracting gait signatures based on anatomical knowledge,” in *Proceedings of BMVA Symposium on Advancing Biometric Technologies*. Citeseer, 2002, pp. 596–606.

[38] A. Hermans, L. Beyer, and B. Leibe, “In defense of the triplet loss for person re-identification,” *arXiv preprint arXiv:1703.07737*, 2017.

[39] S. Feng, C. Miao, K. Xu, J. Wu, P. Wu, Y. Zhang, and P. Zhao, “Multi-scale attention flow for probabilistic time series forecasting,” *arXiv preprint arXiv:2205.07493*, 2022.

[40] S. Feng, C. Xu, Y. Zuo, G. Chen, F. Lin, and J. XiaHou, “Relation-aware dynamic attributed graph attention network for stocks recommendation,” *Pattern Recognition*, vol. 121, p. 108119, 2022.

[41] C. Su, J. Li, S. Zhang, J. Xing, W. Gao, and Q. Tian, “Pose-driven deep convolutional model for person re-identification,” in *Proceedings of the IEEE International Conference on Computer Vision (ICCV)*, 2017, pp. 3960–3969.

[42] L. Wei, S. Zhang, H. Yao, W. Gao, and Q. Tian, “GLAD: Global-local-alignment descriptor for pedestrian retrieval,” in *Proceedings of the 25th ACM international conference on Multimedia*, 2017, pp. 420–428.

[43] T. Wang, H. Liu, P. Song, T. Guo, and W. Shi, “Pose-guided feature disentangling for occluded person re-identification based on transformer,” in *Proceedings of the AAAI Conference on Artificial Intelligence (AAAI)*, vol. 36, no. 3, 2022, pp. 2540–2549.

[44] J. Lu, H. Wan, P. Li, X. Zhao, N. Ma, and Y. Gao, “Exploring high-order spatio-temporal correlations from skeleton for person re-identification,” *IEEE Transactions on Image Processing*, 2023.

[45] J. Liu, B. Ni, Y. Yan, P. Zhou, S. Cheng, and J. Hu, “Pose transferrable person re-identification,” in *Proceedings of the IEEE conference on Computer Vision and Pattern Recognition (CVPR)*, 2018, pp. 4099–4108.

[46] Z. Wu, Y. Xiong, S. X. Yu, and D. Lin, “Unsupervised feature learning via non-parametric instance discrimination,” in *Proceedings of the IEEE Conference on Computer Vision and Pattern Recognition (CVPR)*, 2018, pp. 3733–3742.

[47] A. van den Oord, Y. Li, and O. Vinyals, “Representation learning with contrastive predictive coding,” *arXiv preprint arXiv:1807.03748*, 2018.

[48] K. He, H. Fan, Y. Wu, S. Xie, and R. Girshick, “Momentum contrast for unsupervised visual representation learning,” in *Proceedings of the IEEE Conference on Computer*

Vision and Pattern Recognition (CVPR), 2020, pp. 9729–9738.

[49] T. Chen, S. Kornblith, M. Norouzi, and G. Hinton, “A simple framework for contrastive learning of visual representations,” in *International Conference on Machine Learning (ICML)*, 2020, pp. 1597–1607.

[50] X. Chen and K. He, “Exploring simple siamese representation learning,” in *Proceedings of the IEEE Conference on Computer Vision and Pattern Recognition (CVPR)*, 2021, pp. 15750–15758.

[51] J. Li, P. Zhou, C. Xiong, and S. Hoi, “Prototypical contrastive learning of unsupervised representations,” in *International Conference on Learning Representation (ICLR)*, 2021.

[52] T. Xiao, S. Liu, S. De Mello, Z. Yu, J. Kautz, and M.-H. Yang, “Learning contrastive representation for semantic correspondence,” *International Journal of Computer Vision*, vol. 130, no. 5, pp. 1293–1309, 2022.

[53] M. Gutmann and A. Hyvärinen, “Noise-contrastive estimation: A new estimation principle for unnormalized statistical models,” in *International Conference on Artificial Intelligence and Statistics*, 2010, pp. 297–304.

[54] W. Ge, “Deep metric learning with hierarchical triplet loss,” in *Proceedings of the European Conference on Computer Vision (ECCV)*, 2018, pp. 269–285.

[55] Q. Hu, X. Wang, W. Hu, and G.-J. Qi, “Adco: Adversarial contrast for efficient learning of unsupervised representations from self-trained negative adversaries,” in *Proceedings of the IEEE Conference on Computer Vision and Pattern Recognition (CVPR)*, 2021, pp. 1074–1083.

[56] W. Wang, W. Zhou, J. Bao, D. Chen, and H. Li, “Instance-wise hard negative example generation for contrastive learning in unpaired image-to-image translation,” in *Proceedings of the IEEE International Conference on Computer Vision (ICCV)*, 2021, pp. 14020–14029.

[57] Y. Kalantidis, M. B. Sariyildiz, N. Pion, P. Weinzaepfel, and D. Larlus, “Hard negative mixing for contrastive learning,” *Advances in Neural Information Processing Systems (NeurIPS)*, vol. 33, pp. 21798–21809, 2020.

[58] V. Verma, T. Luong, K. Kawaguchi, H. Pham, and Q. Le, “Towards domain-agnostic contrastive learning,” in *International Conference on Machine Learning (ICML)*. PMLR, 2021, pp. 10530–10541.

[59] S. Zhang, M. Liu, J. Yan, H. Zhang, L. Huang, X. Yang, and P. Lu, “M-mix: Generating hard negatives via multi-sample mixing for contrastive learning,” in *Proceedings of the 28th ACM SIGKDD Conference on Knowledge Discovery and Data Mining*, 2022, pp. 2461–2470.

[60] J. Robinson, C.-Y. Chuang, S. Sra, and S. Jegelka, “Contrastive learning with hard negative samples,” in *International Conference on Learning Representations (ICLR)*, 2021.

[61] S. Jeon, D. Min, S. Kim, and K. Sohn, “Mining better samples for contrastive learning of temporal correspondence,” in *Proceedings of the IEEE Conference on Computer Vision and Pattern Recognition (CVPR)*, 2021, pp. 1034–1044.

[62] F. Schroff, D. Kalenichenko, and J. Philbin, “Facenet: A unified embedding for face recognition and clustering,” in *Proceedings of the IEEE conference on Computer Vision and Pattern Recognition (CVPR)*, 2015, pp. 815–823.

[63] D. A. Winter, *Biomechanics and motor control of human movement*. John Wiley & Sons, 2009.

[64] M. P. Murray, A. B. Drought, and R. C. Kory, “Walking patterns of normal men,” *Journal of Bone and Joint Surgery*, vol. 46, no. 2, pp. 335–360, 1964.

[65] M. Ester, H.-P. Kriegel, J. Sander, X. Xu *et al.*, “A density-based algorithm for discovering clusters in large spatial databases with noise,” in *ACM SIGKDD Conference on Knowledge Discovery and Data Mining (KDD)*, vol. 96, no. 34, 1996, pp. 226–231.

[66] J. T. Zhou, S. J. Pan, and I. W. Tsang, “A deep learning framework for hybrid heterogeneous transfer learning,” *Artificial Intelligence*, vol. 275, pp. 310–328, 2019.

[67] B. Sun, J. Feng, and K. Saenko, “Return of frustratingly easy domain adaptation,” in

Proceedings of the AAAI Conference on Artificial Intelligence (AAAI), vol. 30, no. 1, 2016, pp. 2058–2065.

[68] A. Vaswani, N. Shazeer, N. Parmar, J. Uszkoreit, L. Jones, A. N. Gomez, L. Kaiser, and I. Polosukhin, “Attention is all you need,” *Advances in Neural Information Processing Systems (NeurIPS)*, vol. 30, 2017.

[69] A. Nambiar, A. Bernardino, J. C. Nascento, and A. Fred, “Context-aware person re-identification in the wild via fusion of gait and anthropometric features,” in *International Conference on Automatic Face & Gesture Recognition*. IEEE, 2017, pp. 973–980.

[70] M. Munaro, S. Ghidoni, D. T. Dizmen, and E. Menegatti, “A feature-based approach to people re-identification using skeleton keypoints,” in *International Conference on Robotics and Automation (ICRA)*. IEEE, 2014, pp. 5644–5651.

[71] S. Yu, D. Tan, and T. Tan, “A framework for evaluating the effect of view angle, clothing and carrying condition on gait recognition,” in *International Conference on Pattern Recognition (ICPR)*, vol. 4. IEEE, 2006, pp. 441–444.

[72] Z. Liu, Z. Zhang, Q. Wu, and Y. Wang, “Enhancing person re-identification by integrating gait biometric,” *Neurocomputing*, vol. 168, pp. 1144–1156, 2015.

[73] L. Zheng, L. Shen, L. Tian, S. Wang, J. Wang, and Q. Tian, “Scalable person re-identification: A benchmark,” in *Proceedings of the IEEE International Conference on Computer Vision (ICCV)*, 2015, pp. 1116–1124.

[74] K. Q. Weinberger and L. K. Saul, “Distance metric learning for large margin nearest neighbor classification.” *Journal of Machine Learning Research*, vol. 10, no. 2, pp. 207–244, 2009.

[75] J. V. Davis, B. Kulis, P. Jain, S. Sra, and I. S. Dhillon, “Information-theoretic metric learning,” in *International Conference on Machine Learning (ICML)*, 2007, pp. 209–216.

[76] D. Gray and H. Tao, “Viewpoint invariant pedestrian recognition with an ensemble of localized features,” in *Proceedings of the European Conference on Computer Vision (ECCV)*. Springer, 2008, pp. 262–275.

[77] M. Farenzena, L. Bazzani, A. Perina, V. Murino, and M. Cristani, “Person re-identification by symmetry-driven accumulation of local features,” in *Proceedings of the IEEE Conference on Computer Vision and Pattern Recognition (CVPR)*. IEEE, 2010, pp. 2360–2367.

[78] Z. Cao, G. Hidalgo, T. Simon, S.-E. Wei, and Y. Sheikh, “OpenPose: realtime multi-person 2D pose estimation using part affinity fields,” *IEEE Transactions on Pattern Analysis and Machine Intelligence*, vol. 43, no. 1, pp. 172–186, 2019.

[79] C.-H. Chen and D. Ramanan, “3D human pose estimation= 2D pose estimation+ matching,” in *Proceedings of the IEEE Conference on Computer Vision and Pattern Recognition (CVPR)*, 2017, pp. 7035–7043.

[80] L. Van der Maaten and G. Hinton, “Visualizing data using t-SNE.” *Journal of Machine Learning Research*, vol. 9, no. 11, pp. 2579–2605, 2008.